
# Effects of Weathering on the Properties of Vinyl Siding

Course No: T02-010
Credit: 2 PDH

Roman Titov, P.E., C.C.M., LEED AP.

Continuing Education and Development, Inc.

P: (877) 322-5800
info@cedengineering.com

*This course was adapted from the NIST U.S. Department of Commerce, Publication No. NIST TN 2304, "Effects of Weathering and Formulation on the Properties of Vinyl Siding", which is in the public domain.*

**Abstract**

Vinyl siding has become popular for residential exteriors across the United States. In its insulated form, this siding includes a vinyl shell, capstock, and substrate that encase a foamed material, serving as an efficient insulating material. Despite offering a cost-effective solution with numerous benefits such as improved energy efficiency, straightforward installation, noise reduction, intrinsic low flammability, aesthetic appeal, minimal maintenance needs, durability, and protection against environmental factors like humidity and mold, there are two critical areas for potential improvement. Firstly, its durability can be compromised by exposure to sun, heat, rain, wind, dust, and pollutants, which may lead to the degradation and cracking of the shell, thus affecting its effectiveness as a protective exterior layer. Secondly, fire performance is a concern, especially when vinyl siding is used in its insulated form or installed over flammable foam insulation. The 2021 International Energy Conservation Code (IECC) introduced a requirement for exterior continuous insulation for residential buildings in most U.S. territories (climate zone 4 and above) when following the prescriptive compliance option. Some insulating materials, such as foamed polystyrene or specific grades of polyurethane spray foams, are highly flammable. In the event of a fire, a vinyl shell, which can act as an external fire barrier preventing or delaying ignition of the foamed insulation, is desirable to inhibit fire rapid growth. This feature is increasingly vital due to the prevalence of wildland-urban interface (WUI) fires. Although vinyl siding, based on unplasticized polyvinyl chloride (U-PVC), inherently exhibits flame-retardant properties, it might not be an effective fire barrier. This limitation could arise from issues like melting or possible weathering-induced cracking of vinyl siding.

This study investigated (1) the weathering of commercial vinyl siding and (2) the impact of various additives (impact modifiers, titanium dioxide, calcium carbonate, and stabilizers) on the mechanical performance of U-PVC formulations before and after weathering. The color and gloss retention, mechanical properties, and surface chemistry after weathering were also studied to understand which additives affected the item's weatherability more. Weathering experiments were conducted using a Q-Lab accelerated weathering tester (QUV), simulated photodegradation via high energy radiant exposure (SPHERE), and natural outdoor exposure in Florida. Mechanical properties were assessed through tensile and impact strength tests, while chemical properties were analyzed via Fourier-transformed infrared (FTIR) spectroscopy. Aging effects on color and gloss were also monitored. The impact of additives and weathering on flammability was also studied with two tests: micro combustion calorimetry (MCC) and a recently adopted test based on cone calorimetry (ASTM E3367), which was explicitly performed to evaluate the ability of the siding materials to act as a fire barrier.

Regarding durability, the results revealed that the content of titanium dioxide and calcium carbonate significantly influenced the weatherability of the siding due to its chemical nature and interactions with the PVC matrix. Regarding fire performance, MCC revealed a significant effect of various additives but a low to insignificant impact of weathering. In particular, the formulation with the highest calcium carbonate content performed best in MCC. Noticeably, all

U-PVC formulations - within the limited set investigated in this study - failed to act as an effective fire barrier, exposing the insulation foam underneath due to melting, flowing, and shrinking of U-PVC during combustion.

**Keywords**

Environmental degradation; kinetics; photo-degradation; poly(vinyl)chloride; PVC; reciprocity; weatherability.

## Table of Contents



## List of Tables

## List of Figures

## NIST Disclaimer

Identifying any commercial product or trade name does not imply endorsement or recommendation by NIST. The policy of NIST is to use metric units of measurement in all its publications and to provide statements of uncertainty for all original measurements. In this document, however, data from organizations outside NIST are shown, which may include measurements in non-metric units or measurements without uncertainty. Unless otherwise specified, the uncertainties shown are equal to +/- one standard deviation.

## Author Contributions

**Author 1 (Lankone)**: Conceptualization, Methodology, Data curation/analyses Writing-Original draft preparation. **Author 2 (Zammarano)**: Conceptualization, Methodology, software, Reviewing and Editing. **Author 3 (Jhang)**: Data curation/analysis **Author 4 (Kim)**: Data curation, Writing-Original Draft Preparation. **Author 5 (Goodwin)**: Methodology, Data analysis,

Visualization, Reviewing and Editing. **Author 6 (Kuo):** Data curation/analyses. **Author 7 (Sarti):** Conceptualization, Data curation, writing, Supervision. **Author 8 (Gardi):** Conceptualization, Writing. **Author 9 (Cardelli):** Conceptualization, Formulation**,** Validation. **Author 10 (Sung)**: Conceptualization, Writing-Reviewing and Editing, Supervision.

# 1. Introduction

## 1.1. Vinyl siding and research objectives

According to the Energy Information Agency (EIA) of the United States Department of Energy, the average U.S. household commits nearly half (52 %) of its total energy consumption to heating and cooling [1]. Thus, improving home insulation can have a measurable impact on overall U.S. energy demand. In 2021, the International Energy Conservation Code (IECC) mandated the inclusion of exterior continuous insulation for walls across much of the United States - specifically in IECC climate zone 4 and above - when following the prescriptive compliance option in residential buildings [2]. IECC has also introduced similar requirements for commercial buildings [2]. Exterior insulation can include highly flammable foam materials like polystyrene foams [3, 4]. Non-combustible exterior insulation materials like mineral wool offer an alternative, albeit at a higher cost. When exposed to an ignition source, polystyrene and polyurethane foams, and, to a lesser extent, polyisocyanurate foams can catch fire and accelerate flame spread throughout the entire structure [5]. The importance of this vulnerability is expected to grow in the future, driven by the rapid increase in both the severity and frequency of wildland-urban interface (WUI) fires [6]. This issue is particularly notable in the Northeast and Midwest regions of the U.S., where vinyl siding is the predominant exterior material for residential buildings, and the 2021 IECC mandates the use of exterior insulation when following the prescriptive compliance option [2, 7].

Vinyl siding is a cladding material for exterior walls. It is primarily composed of unplasticized polyvinyl chloride (U-PVC). It was introduced into the U.S. market in the late 1950s, gradually replacing wood, aluminum, or fiber-cement clapboard. Vinyl siding manufacturing involves the co-extrusion of two layers: (1) the substrate layer, which is based on a low-cost U-PVC compound, and (2) the "weatherable capstock," a thin outer layer enriched in titanium dioxide ($TiO_2$), which is composed of either U-PVC, poly(methyl methacrylate) (PMMA), acrylonitrile styrene acrylate (ASA) or blends of these materials. Additional additives are incorporated into U-PVC compounds used for substrates or capstocks to aid in processing and shaping, lower costs, and achieve specific final characteristics such as weather resistance, fire performance, color, aesthetics, and mechanical properties. In the case of insulated vinyl siding, a layer of foam insulation (usually expanded polystyrene or polyisocyanurate) is included beneath the vinyl shell.

Vinyl siding typically exhibits a low flammability thanks to the properties of its main component, polyvinyl chloride (PVC). PVC is an inherently flame retarded polymer with a favorable combination of ease of extinguishment, low heat release rate, ignitability, and flame spread rate [5, 8, 9]. While PVC is a low-cost commodity polymer akin to polyethylene, polypropylene, and polystyrene, it possesses a significantly lower flammability. For comparison, the fire growth capacity (a fundamental property measured by ASTM D7309 that correlates with a material's flammability [10, 11]) is 1078 J/(g · K) for polyethylene, 836 J/(g · K) for polypropylene and 88 J/(g · K) for PVC [12].

In this study, the effects of weathering were investigated on (1) commercial vinyl siding with an ASA capstock sourced from the U.S. and (2) vinyl siding formulations developed explicitly for this research (R&DFs), wherein additives such as light and thermal stabilizers, impact modifiers, titanium dioxide ($TiO_2$) and fillers were systematically adjusted. Specimens from both groups were exposed to natural and accelerated weathering to evaluate the effect of these additives during weathering. Following weathering exposure, samples were retrieved for extensive characterization as appearance (color/gloss) measurements, Fourier Transform Infrared Spectroscopy (FTIR), laser scanning confocal microscopy (LSCM), scanning electron microscopy (SEM), and mechanical testing. These analyses aimed to monitor the polymer degradation rate and the overall deterioration of siding performance.

The fire performance of U-PVC compounds was assessed by Microscale Combustion Calorimetry (MCC), according to ASTM D7309 method A [10], and a modified cone calorimeter test - ASTM E3367 [13].
MCC was used to measure the heat release rate of each U-PVC formulation by pyrolyzing specimens in nitrogen and then oxidizing the pyrolizates in a combustion chamber at 900 °C [12, 14, 15]. While MCC does not match any specific fire test scenario and does not consider extrinsic factors (like heat irradiance, ventilation, shape, size, and density of the specimen), it measures intrinsic material properties (i.e., properties depending solely on the chemical structure of the material) relevant to flammability. Despite its limitations, MCC has effectively predicted a material's likelihood to meet fire test requirements. For instance, the fire growth capacity (FGC) measured in MCC has been used to predict the outcome of tests like UL 94 V and 14 CFR 25 [11, 12].

As previously noted, vinyl siding is expected to exhibit low flammability. Yet, its effectiveness as a fire barrier requires further validation, and it may be compromised by factors such as embrittlement and cracking in weathered samples. ASTM E3367 is a recent test developed to assess the combustion behavior of layered assemblies, such as those found in upholstered furniture [16, 17]. Herein, this test was used to evaluate the ability of vinyl siding to shield a flammable substrate, such as polystyrene foam, by acting as a protective barrier.

### 1.2. Weathering of acrylic-based polymers

PMMA and ASA-based capstock are commonly used as protective layers due to their optical clarity, absence of color, and ease of application. Typically, they contain at least 10 % by mass of $TiO_2$, which shields the polymer matrix from UV-induced degradation. PMMA and ASA weathering have been extensively discussed elsewhere [18-20]. Briefly, the $TiO_2$-rich polymers primarily degrade via photo-degradation in areas where oxygen is depleted, and $TiO_2$ initiates photo-oxidation in regions where oxygen is available. Both processes lead to chain scission in the polymer backbone, resulting in decreased mechanical properties, color alteration, and gloss reduction.

### 1.3. Thermal degradation and weathering of PVC

When exposed to heat, PVC undergoes thermal degradation. This degradation involves sequentially eliminating hydrogen chloride (HCl) from allylic chlorine and forming polyene sequences. This process, catalyzed by HCl and Lewis acids, operates through an ionic mechanism [21]. Allylic chlorine is also the target of photochemical reactions during weathering.

Extensive studies by various authors, mainly in the 1980s and 1990s, have detailed the weathering of PVC [22-28]. Weathering of U-PVC is a complex phenomenon that involves photo-degradation, photo-oxidation, photo-catalyzed oxidation, photobleaching, thermal degradation, and other chemical reactions. Weathering of PVC results from photon-induced reactions on the material's surface. These reactions, with or without oxygen and water, lead to mechanical and aesthetic issues such as loss of mechanical properties, yellowing, and chalking. Dark-colored U-PVC articles, reaching temperatures over 70 °C, may undergo simultaneous light-induced and thermal degradation.

During the weathering of PVC compounds, chemical reactions on the surface lead to the formation of three layers [25, 26]. The first is the oxidized layer, where photo- and photo-catalyzed oxidation are the dominant reactions; its thickness depends on $TiO_2$ concentration, grade, and oxygen diffusion. The second is a colored layer with a high molar extinction coefficient, containing polyene sequences (generated by photo-degradation) and condensation products. The third one is the undegraded core, whose degradation is prevented by the protective action of the second layer.

Because U-PVC is transparent at wavelengths below 250 nm, the initiation of these processes is likely caused by chromophores present in the resins or generated during product manufacturing. These chromophores absorb UV radiation, leading to the degradation and alteration of the chemical structure of the U-PVC compound over time, which can result in changes in color, strength, and other properties. Hydroperoxides and ketones are typical chromophores found in U-PVC., When exposed to light irradiation, they generate radicals through a Norrish type I reaction [22].

Polyene sequences can be formed during the PVC resin synthesis or the U-PVC compound processing. Due to their high extinction coefficient, polyenes rapidly become the main absorbing chromophores. Only polyene sequences containing more than four units interact significantly with sunlight. Sunlight reaching the Earth's surface is filtered by the atmosphere, and wavelengths shorter than 290 nm are mostly absorbed. Consequently, sunlight does not affect polyene sequences with four or fewer units. In comparison, those with more than four units absorb light in the range of wavelengths that penetrate the atmosphere, contributing to the photochemical degradation and weathering of PVC materials [21] [29]. The interaction between light and polyene generates an excited singlet state of polyene, which deactivates via both radiative and non-radiative pathways. In one of the non-radiative pathways, a chlorine

radical is released· Cl from allylic chlorine leads to the formation of polyene sequences, HCl, crosslinking, and chain scission products, as previously described [22].

This pathway rapidly releases Cl before oxygen can quench the excited singlet polyene, a process known as photo-degradation. Importantly, photo-degradation can occur both in the presence and absence of oxygen. However, the second radical formed from deactivating the excited singlet polyene has a longer lifetime, allowing it to react with oxygen. This initiates a series of reactions responsible for the photooxidation of the matrix, including chain scission and the formation of carbonyl and carboxyl groups. The prevalence of photo-degradation occurs in areas where oxygen is limited, such as beneath the surface. Conversely, photo-oxidation prevails in regions near the surface where oxygen can readily diffuse, facilitating reactions with the radicals generated by the excited singlet polyene [25].

Common additives found in the U-PVC compound can further complicate the weathering pattern. For example, titanium dioxide ($TiO_2$) is a standard pigment and light stabilizer for outdoor PVC items. $TiO_2$ grades for PVC are surface-treated with $SiO_2$, $Al_2O_3$, and zirconium to reduce their photocatalytic activity. In this way, their unique ability to adsorb most UV light impedes a deeper penetration of the photons and protects the bulk matrix from degradation. Even with a coating, $TiO_2$ retains enough residual photocatalytic activity to facilitate surface oxidation, leading to bleaching and chalking, particularly in the presence of water [30]. Experimental results indicate that direct contact with water, such as from condensation or rain, leads to more severe degradation than conditions with high air humidity.

Furthermore, fillers commonly used in PVC articles can influence the degradation and chalking of weathered PVC items. For example, calcium carbonate reacts with HCl and yields calcium dichloride, which, being hydrophilic and water-soluble, increases oxygen concentration in the matrix, thus promoting photo- and photo-catalyzed oxidation. Photo-catalyzed oxidation, photo-oxidation, photo- and thermal-degradation, and chemical reactions leading to the formation of water-soluble and hydrophilic molecules are responsible for the surface disintegration of the polymeric matrix in outdoor applications. As a result, free particles of $TiO_2$ and other fillers are released, and microcracks or holes become visible on the surface as faded and chalked areas. Eventually, the disintegration of the polymeric shell matrix exposes the U-PVC substrate to light and oxygen. Polyene sequences are oxidized through photobleaching (which leads to shorter polyene sequences), and photo- or photo-catalyzed oxidation perpetuates the erosion process deeper into the material.

### 1.4. Polymer decomposition and combustion

As a thin layer, the PMMA or ASA capstock assumes a secondary role in fire performance compared to the U-PVC substrate. The initial stage of the thermal decomposition in PVC occurs between 220 °C and 350 °C, where HCl is released in the gas phase - leaving polyene sequences, their condensation products, and unsubstituted aromatic hydrocarbons in the gas phase. In the subsequent stage, above 450 °C, primarily aliphatic hydrocarbons are released, and a

carbonaceous char is formed from the condensation products of polyene sequences. The decomposition pathway and release of flammable pyrolyzates are further complicated by additives in PVC compounds. Detailed information on the decomposition and combustion of PVC-based formulations is available elsewhere [31-34].

## 2. Materials and Methods

### 2.1. Materials, formulations, and sample preparation

A commercial insulated vinyl siding was purchased in the U.S. The siding complies with ASTM D7793, which defines requirements for thermal insulation, warp and shrinkage resistance, impact strength, appearance, thermal distortion resistance, flame spread, and wind-load resistance [35]. The vinyl shell consists of rich $TiO_2$ ASA capstock and U-PVC substrate, while the insulation material is expanded foamed polystyrene (EPS).

R&DFs were also prepared (Table 1). Table 1 shows the type, trade name, manufacturer, CAS #, and mass of raw material required to prepare 100 g of a given R&DF.

**Table 1. Type, trade name, manufacturer, CAS#, and mass of raw material required to prepare a given R&DF.**

| Raw Materials | Trade name | Manufacturer | CAS # | A ref [g] | C [g] | F [g] | H [g] |
|---|---|---|---|---|---|---|---|
| PVC | PVC 264GC | Inovyn, UK | 09002-86-2 | 85 | 85 | 85 | 85 |
| PVC | PVC S5745 | Inovyn, UK | 09002-86-2 | 15 | 15 | 15 | 15 |
| $CaCO_3$ coated | VALTOCHIM | Umbria Filler, Italy | 00471-34-1 | 15 | 15 | 15 | 30 |
| Acrylic impact modifier | KANE ACE FM 50 | Kaneka, Belgium | | 2.5 | 2.5 | 7.5 | 7.5 |
| Chlorinated polyethylene | CPE 6135 | R.G. chem, Italy | 64754-90-1 | 2.5 | 2.5 | - | - |
| Processing aids | REAMOD P 220 | Reagens, Italy | - | 0.5 | 0.5 | 0.5 | 0.5 |
| $TiO_2$ | TRONOX CR 826 | Tronox, U.S. | 1317-80-2 | 1.0 | 7.5 | 7.5 | 7.5 |
| Tin stabilizer | REA. TIN. OR 860 | Reagens, Italy | 68109-88-6 | 2.5 | - | - | - |
| Calcium stearate | ARESTAB CA | Reagens, Italy | 1592-23-0 | 1.0 | - | - | - |
| Polyethylene wax | REALUBE PO | Reagens, Italy | 9002-88-4 | 0.5 | - | - | - |
| Internal lubricant | REALUBE SD | Reagens, Italy | 90193-76-3 | 0.6 | 0 | 0 | 0 |
| Calcium zinc stabilizer | RPK B-AV/2140 | Reagens, Italy | - | - | 4.0 | 4.0 | 4.0 |

In the U.S. market, the U-PVC substrate formulations are usually stabilized with di alkyl tin mercapto alcohol esters (also known as alkyltin "reverse esters"), dosed at (0.4 to 0.8) % by mass. This class of stabilizer is not registered in the European Union (EU) and, therefore, is not used in this research. Instead, an alkyl tin carboxylate stabilizer, dioctyl bis-(ethyl maleate), CAS number 68109-88-6, was utilized.

The blends of Table 1 were prepared in a turbo mixer (model RV/10/20/FV, Plas Mec) with a maximum processing temperature of 105 °C. The dry blends were cooled to room temperature and calendered at 180 °C for 3 min to form polymer sheets. The sheets were hot pressed at 180 °C per 5 min at 150 atm and cooled at room temperature to produce 1.1 mm thick plaques. Test specimens for tensile-impact test and weathering were obtained from the plaques.

## 2.2. Weathering

The vinyl shell underwent accelerated and natural outdoor weathering, whereas R&DF was exposed only to accelerated weathering. Following ASTM G7/G7M [36] procedures, the outdoor exposure occurred at a weathering site near Homestead, Florida (U.S.). Samples were exposed from October 21, 2020, to April 21, 2022 (18 months). During this time, the daily mean temperature measured on the sample backside was (27 ± 7) °C. The average daily UV dose, calculated between 300 nm and 385 nm, was (0.84 ± 0.11) MJ/m$^2$, and the cumulative UV irradiance for 12 months was approximately 302 MJ/m$^2$. Finally, the average relative humidity was (76 ± 7) % RH. Dogbone-shaped samples were prepared for mechanical and impact testing by cutting samples with a punch die Type V [37]. Long rectangular sheet samples were utilized for chemical characterizations.

Accelerated laboratory exposures were carried out at NIST in the simulated photodegradation via high energy radiant exposure (SPHERE) [36, 38, 39], and a Q-Lab accelerated weathering tester (QUV SOLAR EYE, Q-LAB Corporation, Westlake, OH, U.S.), referred to as QUV-1. A parallel weathering test was performed at Reagens S.p.A. on a QUV-2, which is like the QUV-1. QUV weathering in presence of UV and water condensation was conducted following cycle 1 in ASTM G154-23 [40]. It consists of 8 hours of UV exposure (340 nm at 0.89 W/m²) at 60 °C, followed by 4 hours of darkness at 50 °C for water condensation. This testing regimen was carried out for up to 12 weeks.

In the NIST SPHERE, temperature and relative humidity (RH) were carefully controlled, and specimens were uniformly exposed to high-intensity UV light, thus accelerating the degradation process compared to outdoor and QUV exposures. The UV irradiance on the samples in the SPHERE is approximately 163 W/m$^2$ between 295 nm and 400 nm. While directly comparing outdoor weathering time is challenging due to the complexity of weather patterns, the equivalent exposure time of one year outdoors in South Florida, with a cumulative UV irradiance of approximately 302 MJ/m², corresponds to roughly 21 days in the SPHERE. Three test conditions were conducted, including 70 °C/70 % relative humidity (RH), 55 °C/75 % RH, and 30 °C/0 % RH. The results presented in this paper mainly focus on the 55 °C/75 % RH exposure conditions. Samples were periodically retrieved for non-destructive characterization using color/gloss meters to monitor changes in appearance (color shift and yellowing index) and Fourier transform infrared spectroscopy in attenuated total reflection mode (ATR-FTIR) to track chemical degradation in the top 2 μm of the surface. Destructive tests, such as tensile and impact testing, were also performed to evaluate the mechanical properties of the SPHERE- and QUV-exposed samples. Table 2 details the weathering type, daily dose, test conditions, and test sample geometry.

**Table 2. Details on weathering conditions.**

| Weathering type | Daily dose between (300 and 400) nm ($MJ/m^2$) | Test conditions | Sample geometries |
|---|---|---|---|
| Natural Outdoor (FL, U.S.) | 0.89 | ASTM G7<br>(27 ± 7) °C<br>RH (76 ± 6) % | Dogbone, 1.1 mm thick |
| SPHERE | 14.26 | 163 $W/m^2$ between 300 nm and 400 nm<br>(55 ± 1) °C<br>RH (75 ± 2) % | Dogbone,<br>19 mm diameter disk,<br>1.1 mm thick |
| QUV 1 & 2 | 2.2 | ASTM G154 (Cycle 1)<br>8h exposure (340 nm at 0.89 $w/m^2$) at<br>60 °C + 4 h at 50 °C condensation (no UV) | Dogbone,<br>1.1 mm thick |

## 2.3. Chemical characterization

Fourier-transform infrared spectroscopy with attenuated total reflectance (ATR-FTIR) was performed using a Thermo Scientific Nicolet iS50 FTIR spectrometer featuring a diamond ATR crystal. The spectral range spanned between 3700 $cm^{-1}$ and 600 cm-1, with a resolution set at 0.4 cm-1, 128 scans per specimen, and a measurement depth of approximately 2 μm. The FTIR spectra underwent linear baseline correction, employing identical baseline points across all spectra, and were subsequently normalized by the peak intensity at 611 $cm^{-1}$ (stretching C-Cl).

## 2.4. Mechanical characterization

Tensile tests were performed according to ASTM D638 using an MTS Criterion 45 testing system with a 5 kN load cell and a crosshead speed of 12.7 mm/min [34]. Both unexposed and exposed U-PVC were tested using a dogbone type 5. Elongation-at-break (EaB), yield stress, and elastic modulus were calculated from the uniaxial stress-strain curves of U-PVC. The elongation-at-break data presented in this paper are the average of at least five test samples. Tensile-impact strength was measured on unexposed and exposed dogbone type 2 U-PVC samples using a pendulum impact tester at 7.5 J (model Zwick Roel, HIT5-5P) following ISO 8256, method A [37]. The tensile-impact strength data presented in this paper is the average of at least five test samples.

## 2.5. Surface appearance and morphology characterization

During weathering, samples were removed periodically for characterization using a portable spectrophotometer with integrated gloss measurement (spectro-guide sphere gloss meter, BYK-Gardner U.S., Columbia, MD). The specimen color was evaluated in terms of yellowness

index (YI) according to ASTM E313 and in terms of color shift ΔE calculated according to ASTM D2244 as a function of L* a* b* coordinates defined by the International Commission on Illumination (CIE) [41, 42].

Color shift ΔE was expressed according to equation 1:

$$\mathrm{I}\Delta E = \sqrt{(L^* - L_0^*)^2 + (a^* - a_0^*)^2 + (b^* - b_0^*)^2} \quad (1)$$

All $\Delta E$ and *YI* data are reported as the average of four measurements. Uncertainties are shown as ± one standard deviation (calculated from four measurements on the same specimen). Note that measurement uncertainties for different specimens on the same exposure conditions were less than 2 %, according to previous experiments.

The surface morphology and surface roughness were characterized by laser scanning confocal microscopy (LSCM Zeiss model LSM 800, Thornwood, NY, reflectance mode, 405 nm laser) with 20x/0.7, 150x/0.95 air lens at scanning z-step of 0.1 µm. The root-mean-square (RMS) surface roughness (Sq) values were calculated using Zeiss Confomap software using ISO 25178 standard analysis within a scanning area of 650 µm x 650 µm [43]. Three locations per sample were randomly selected for imaging and topography data collection.

Scanning electron microscopy (SEM) with energy dispersive X-ray spectroscopy (EDX) (JEOL, 7600f, Peabody, MA) was performed to investigate the composition of ASA/$TiO_2$ - capstock and image the surface morphology of degraded U-PVC samples by secondary electron and backscatter emission.

### 2.6. Fire performance

A microscale combustion calorimeter (Deatak MCC-3) was used according to ASTM D7309 to measure the heat release rate of each U-PVC formulation by pyrolyzing a (5.6 ± 0.1) mg specimen in nitrogen at a heating rate of 1°C/s and then oxidizing the pyrolizates in a combustion chamber at 900 °C.

The ability of the U-PVC shell to protect a polystyrene foam substrate was tested according to ASTM E3367. U-PVC sheets with a thickness of (1.1 ± 0.1) mm were cut into 125 mm × 125 mm square samples. Extruded grade polystyrene (XPS) with a nominal density of 30 Kg/$m^3$ and thickness of 25 mm was cut into 100 mm × 100 mm square samples.

The specimen was assembled within the sample holder according to ASTM E3367. The XPS foam was placed inside a 25-mm tall insulated liner (see Fig. 1a); the top surface of the XPS foam was covered by a U-PVC sheet (see Fig. 1b). Notice that the bottom of the sample holder is open and allows the detection of burn through (see Fig. 1c). All tests were run at an external

heat flux of 75 kW/m$^2$. Tests were continued until a burn through was revealed by the ignition of the XPS foam and flame out occurred.

(a)

(b)

(c)

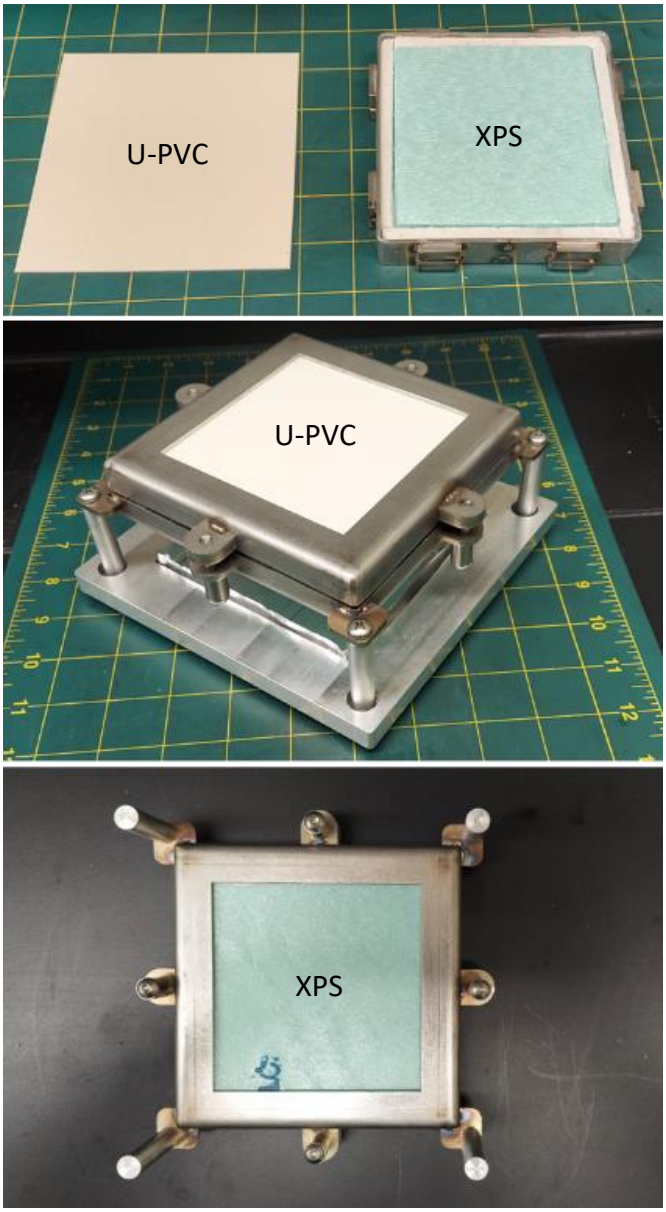


**Fig. 1. Pictures of (a) U-PVC sheet and XPS foam inserted within the insulated liner; (b) sample assembly ready to be tested; (c) detail from the bottom of the sample assembly showing an open design that allows the detection of burn through.**

## 3. Results and discussions

### 3.1. Characterization of the commercial insulated siding

The insulated vinyl siding featured a nominally 1.1 mm-thick vinyl shell and EPS insulation (Fig. 2a). The shell consisted of an approximately 40 µm - thick ASA capstock with high concentration of $TiO_2$ and a U-PVC substrate (Fig. 2b).

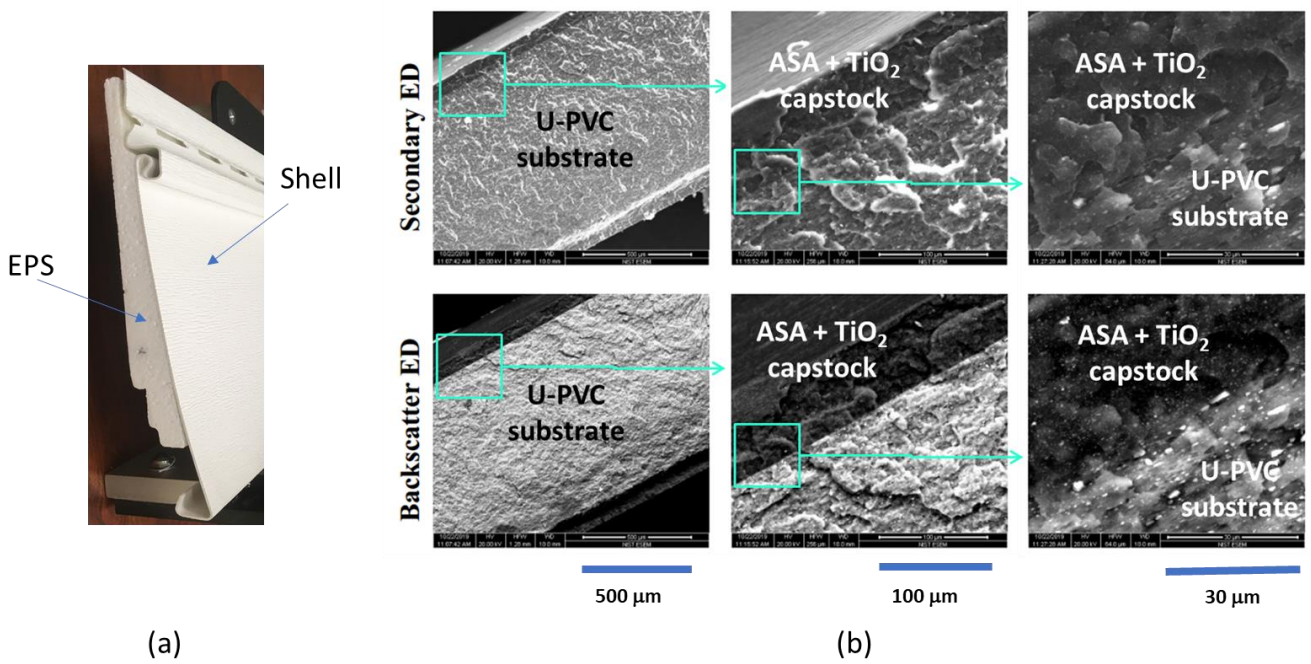


**Fig. 2. Images showing: (a) photo of the commercial vinyl siding and (b) SEM images of the front shell at different scales with both secondary electrons (upper row) and backscattered emission (bottom row).**

Fig. 3 shows the FTIR spectra for all the components of the insulated vinyl siding: the vinyl shell, which includes the ASA capstock with $TiO_2$ (hereafter, **front U-PVC**), U-PVC side in contact with EPS (**back U-PVC**), EPS surface in contact with U-PVC (**front EPS**), and EPS surface on the vinyl siding backside (**back EPS**). The characteristic FTIR peaks for U-PVC (Table 3), ASA compounds (Table 4), and EPS (Table 5) are shown by front U-PVC, back U-PVC, and front/back EPS, respectively.

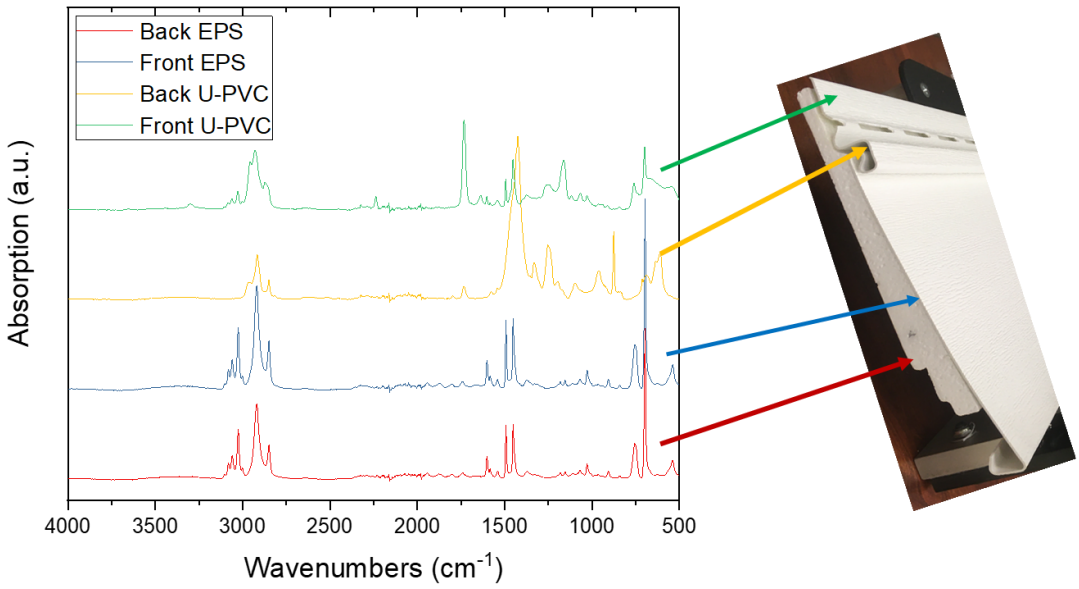


**Fig. 3. FTIR spectra of the component of the vinyl siding.**

**Table 3. Typical FTIR peaks for unexposed U-PVC [44][47].**

| IR band ($cm^{-1}$) | Substance | assignment |
|---|---|---|
| 2972 | PVC | stretching C-H of CHCl |
| 2924 | PVC | Stretching C-H of $CH_2$ |
| 1801 | $CaCO_3$ | Overtone band |
| 1735 | IM | Ester C=O stretch |
| 1431 | $CaCO_3$ | Asymmetric stretching O-C-O |
| 1428 | PVC | Deformation (Wagg) of $CH_2$ - |
| 1332 and 1249 | PVC | Deformation C-H of CHCl |
| 1101 | PVC | Stretching C-C |
| 963 | PVC | Rocking $CH_2$ |
| 875 | $CaCO_3$ | Out of plane vibrations O-C-O |
| 846 | $CaCO_3$ | Out of plane vibrations O-C-O |
| 714 | $CaCO_3$ | Bending O-C-O ] |
| 686,637 and 611 | PVC | Stretching C-Cl |

**Table 4. Typical FTIR peaks for ASA capstock [45, 46].**

| IR band ($cm^{-1}$) | Substance | assignment |
|---|---|---|
| 2239 | ASA | Nitrile CN stretching |
| 1732 | ASA | Ester C=O stretch of butyl acrylate |
| 1602 | ASA | Benzene C-H Stretching |
| 1490 | ASA | Benzene C-H Stretching |
| 1453 | ASA | Benzene C-H Stretching |
| 761 | ASA | Benzene C-H bending out of plane |
| 702 | ASA | Benzene C-H bending out of plane |
| 790 - 400 | $TiO_2$ | Ti-O-Ti Bending and stretching |

**Table 5. Typical FTIR peaks for EPS** [47]**.**

| IR band ($cm^{-1}$) | Substance | assignment |
|---|---|---|
| 3060.8 | PS | Aliphatic C-H Stretching |
| 3026.0 | PS | Aliphatic C-H Stretching |
| 1600.8 | PS | Benzene C-H Stretching |
| 1492.7 | PS | Benzene C-H Stretching |
| 1452.2 | PS | Benzene C-H Stretching |
| 756.0 | PS | Benzene C-H bending out of plane |
| 698.0 | PS | Benzene C-H bending out of plane |

### 3.2.1. Weathering of commercial vinyl siding

The shell of the commercial vinyl siding was subject to three exposure conditions (natural weathering, SPHERE, and QUV) on the front U-PVC, which includes the ASA capstock. Fig. 4 displays the relative FTIR spectra. The unexposed vinyl siding shell exhibits spectroscopic features indicative of an ASA rich in $TiO_2$, as indicated in Table 4. Photo-degradation, photo-oxidation, and photo-catalyzed oxidation by $TiO_2$ (see section 1.3) modified the chemical structure of ASA capstock.

Despite variations in temperature, humidity, and the levels of absorbed energy (dose), all specimens - independent of the exposure condition - exhibited the following features:

- increased intensity in the hydroxyl region (3120 $cm^{-1}$ to 3750 $cm^{-1}$)
- increased intensity in the (790 to 500) $cm^{-1}$ broadband due to Ti-O-Ti bending and stretching;
- decreased intensity in the hydrocarbon region (2700 $cm^{-1}$ to 3000 $cm^{-1}$);
- appearance of a shoulder in the carbonyl region (1600 $cm^{-1}$).

In natural weathering (max dose of 415 MJ/m$^2$) and, more significantly, in the SPHERE (max dose of 1291 MJ/m$^2$), the final exposure dose was higher compared to QUV (max dose of 188.7 MJ/m$^2$). Thus, a more pronounced degradation and modification of the FTIR spectra was observed. This trend is more clearly displayed in Fig. 5, where FTIR spectra from Fig. 4 are shifted to highlight the evolution of selected IR regions as a function of the dose level.

For SPHERE weathering (55 °C, 75 % RH), Fig. 6 displays the IR area as a function of exposure dose in (a) the hydroxyl region (3120 cm$^{-1}$ to 3750 cm$^{-1}$) and (b) the hydrocarbon region (2700 cm$^{-1}$ to 3000 cm$^{-1}$). This is accomplished by first integrating the area under the spectroscopic features corresponding to the hydroxyl and alkyl features, then normalizing the peak area of both features for all exposed samples to the peak areas measured for the unexposed sample. SPHERE and QUV have similar trends in the hydroxyl region and increase faster than FL outdoor. In the hydrocarbon region, the increase rate of QUV > SPHERE > FL outdoors in the exposed dose is less than 400 MJ/m$^2$.

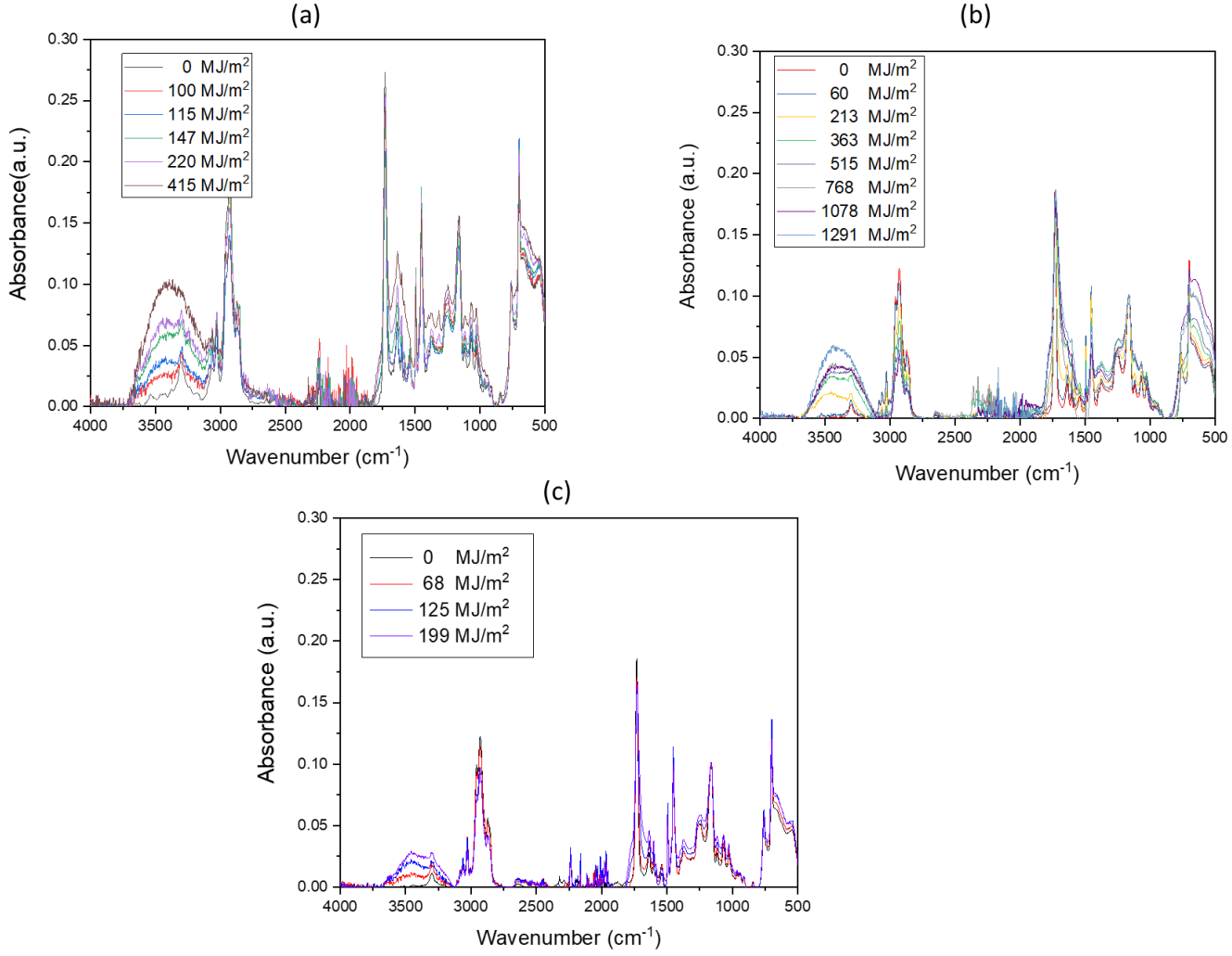


**Fig. 4. FTIR spectra for U-PVC samples exposed to multiple dose levels in: (a) natural weathering, (b) SPHERE, (c) QUV.**

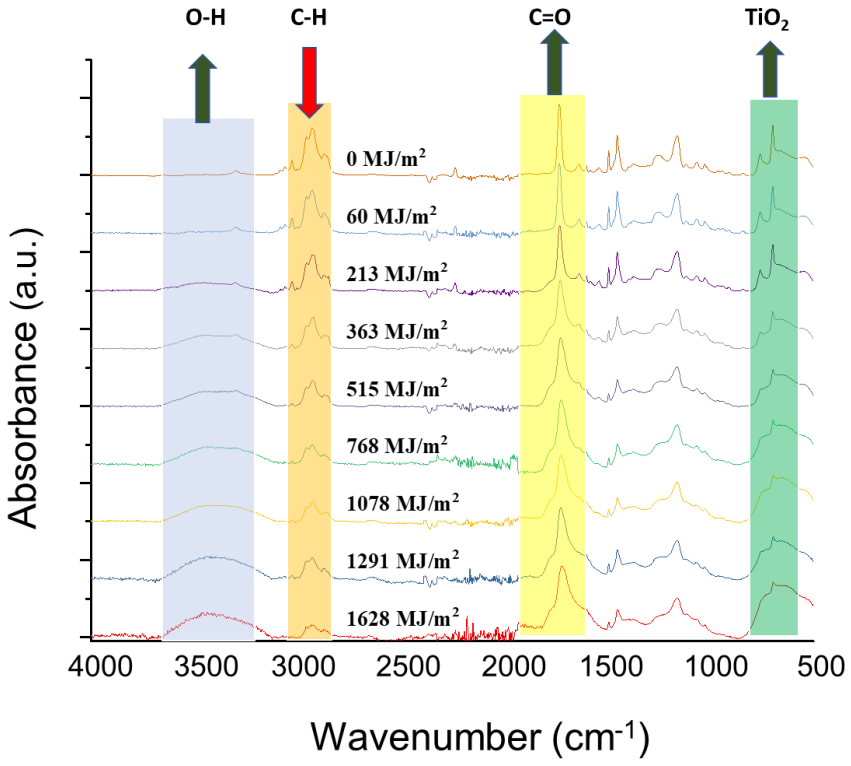


**Fig. 5. Shifted FTIR spectra from Fig. 4b. The evolution of selected IR regions as a function of the dose level are highlighted.**

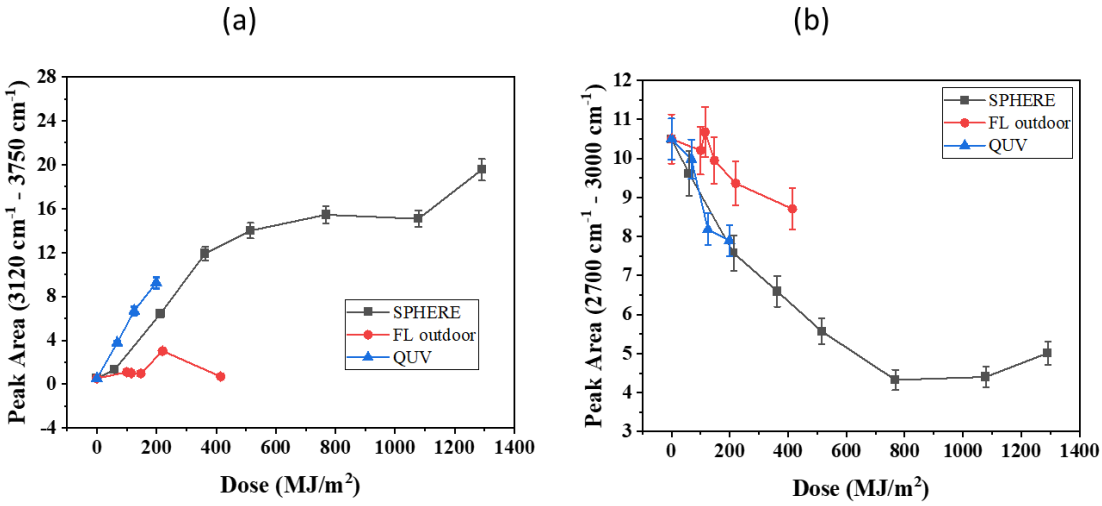


**Fig. 6. IR peak area in the (a) hydroxyl region (3120 cm$^{-1}$ to 3750 cm$^{-1}$) and (b) hydrocarbon region (2700 cm$^{-1}$ to 3000 cm$^{-1}$) as a function of exposure dose in SPHERE (55 °C, 75 % RH), FL outdoor and QUV. Data points indicate the mean and the error bars (± one standard deviation values, calculated over 5 replicate tests).**

### 3.2.2. Surface morphology and appearance

The role of the capstock ($TiO_2$-rich ASA layer) as a weathering protection layer can be demonstrated in the QUV weathering tests, as shown in Fig. 7. There were no significant color changes on the front U-PVC after aging for up to 12 weeks. However, after about four weeks, the back U-PVC side turned yellow/brown.
Fig. 7b displays the corresponding changes in the yellowness index (ΔYI) as a function of exposure weeks in QUV chambers for the front and back surfaces. The values of ΔYI of the back U-PVC at four weeks are much higher than the front (no color change). A significant increase in ΔYI for the front U-PVC face was first observed in week 6.

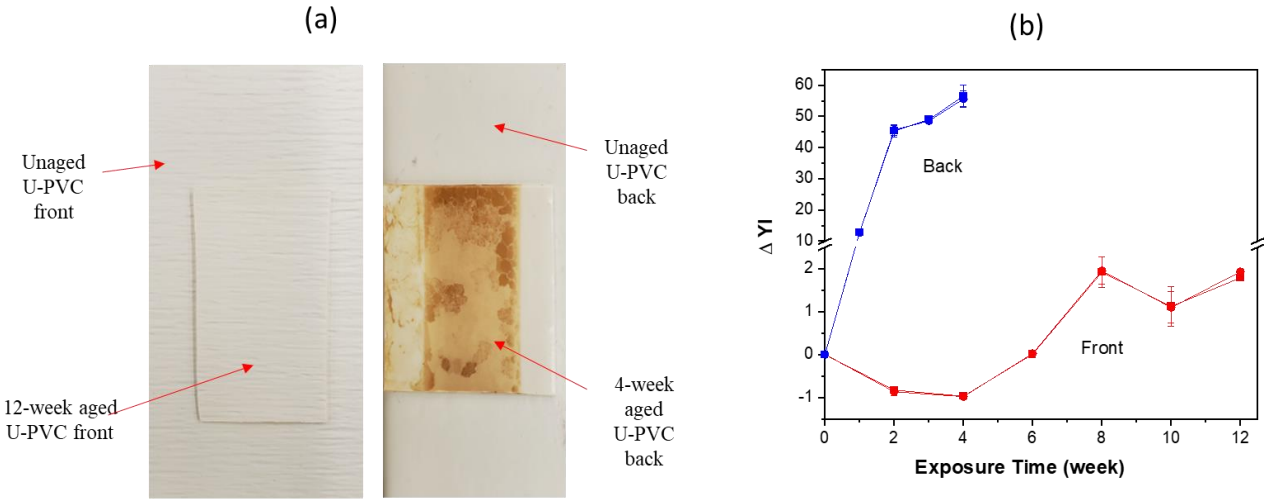


**Fig. 7. (a) Photos of U-PVC surfaces (front and back) before and after QUV aging; (b) corresponding yellowness index (ΔYI) as a function of exposure duration in QUV. Data points indicate the mean, and the error bars the standard deviation (5 replicates).**

Fig. 8 compares the yellowness index (YI) measured on the front U-PVC during weathering in QUV and SPHERE. ΔYI values in QUV are higher than ΔYI in SPHERE. Thus, QUV weathering appears more severe than the SPHERE weathering at a given dose exposure. The primary causes could be water condensation and humidity on the sample surface. Although OH radical production on the $TiO_2$ surface remains relevant (see section 1.3), the primary impact lies in autocatalytic degradation facilitated by hydrochloric acid [48]. The FL outdoor exposed samples (64 weeks, dose up to 415 MJ/m$^2$) showed relatively low color change and some dirt accumulated on the surfaces. This result is mainly attributed to temperature. The average exposure temperature was 27 °C in FL outdoors, 55 °C in SPHERE, and 60 °C in QUV (Table 2). Other factors, such as rain (washing off the photodegradation products), could also affect ΔYI in FL outdoors.

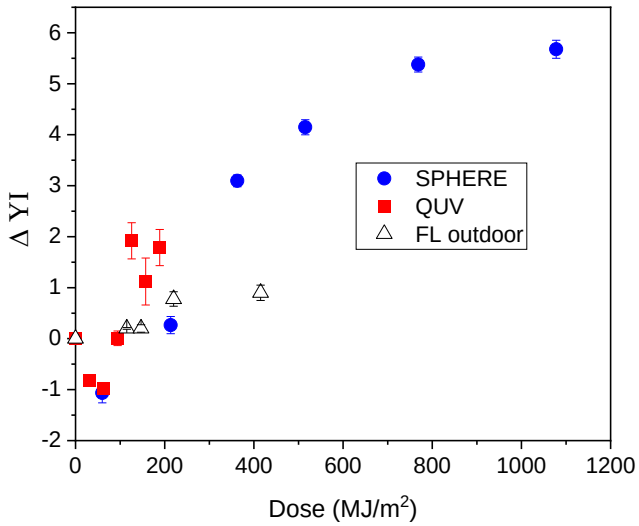


**Fig. 8. Changes in yellowness index (ΔYI) as a function of exposure dose for SPHERE QUV and FL outdoor exposure conditions. Data points indicate the mean and the error bars, the standard deviation values (5 replicates).**

Color appearance measurements using a portable spectrophotometer are commonly used in industrial practice to assess the durability of thermal plastics used in building envelopes. To connect changes in the samples' visual appearance with the changes in chemical structure, color shift (ΔE) and change in yellowing index (ΔYI) were plotted as a function of FTIR calculated areas in the hydroxyl and hydrocarbon regions (Fig. 9) at SPHERE (55 °C, 75 % RH) exposure conditions.

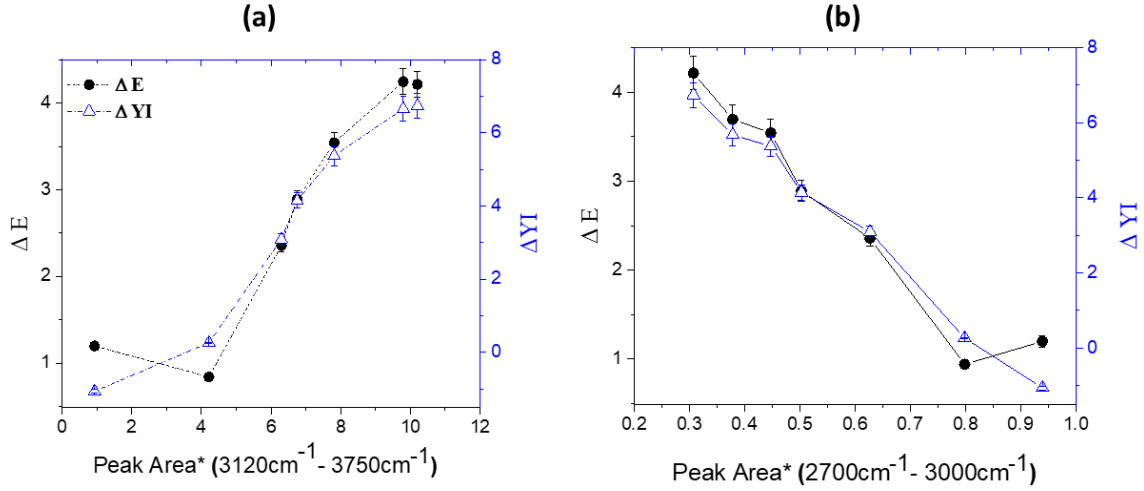


**Fig. 9. Changes in color appearance at SPHERE (55 °C, 75 % RH) exposure conditions vs. changes in IR peak area in (a) hydroxyl region (3120 $cm^{-1}$ to 3750 $cm^{-1}$) and (b) hydrocarbon region (2700 $cm^{-1}$ to 3000 $cm^{-1}$). Peak areas are normalized by the peak area at 0 $MJ/m^2$. Data points indicate the mean and the error bars (one standard deviation, 5 replicates).**

The correlation between color parameters and chemical structure is almost linear in both graphs. These results indicate that E and DYI can be good indicators of U-PVC degradation. The surface morphology of front U-PVC was investigated using LSCM and SEM. Fig. 10 displays the two-dimensional projection of LSCM images (405 nm laser, 150x/0.95 air lens) before exposure (unexposed) and exposed in SPHERE (55 °C, 75 % RH). Due to ASA polymer matrix degradation during weathering, more bright spots, attributed to $TiO_2$, appeared on the surface. The surface roughness (root-mean-square, $S_q$) changed from (0.52 ± 0.06) mm at 0 MJ/m$^2$ (unexposed) to (1.16 ± 0.14) mm at 1628 MJ/m$^2$. SEM and EDX images (Fig. 11 and Fig. 12) indicated degradation/deterioration of the capstock surface (ASA/$TiO_2$) layer after UV exposure and the formation of clusters of $TiO_2$ (Fig. 12). The presence of these clusters, the higher $TiO_2$ IR signals and the collapse of CH stretching bands (see Section 3.2.1 and Fig. 5) are clear evidence of an extensive disintegration of the polymeric matrix leaving widespread areas richer in $TiO_2$. This is a typical behavior in the weathering of polymers containing $TiO_2$ [30].

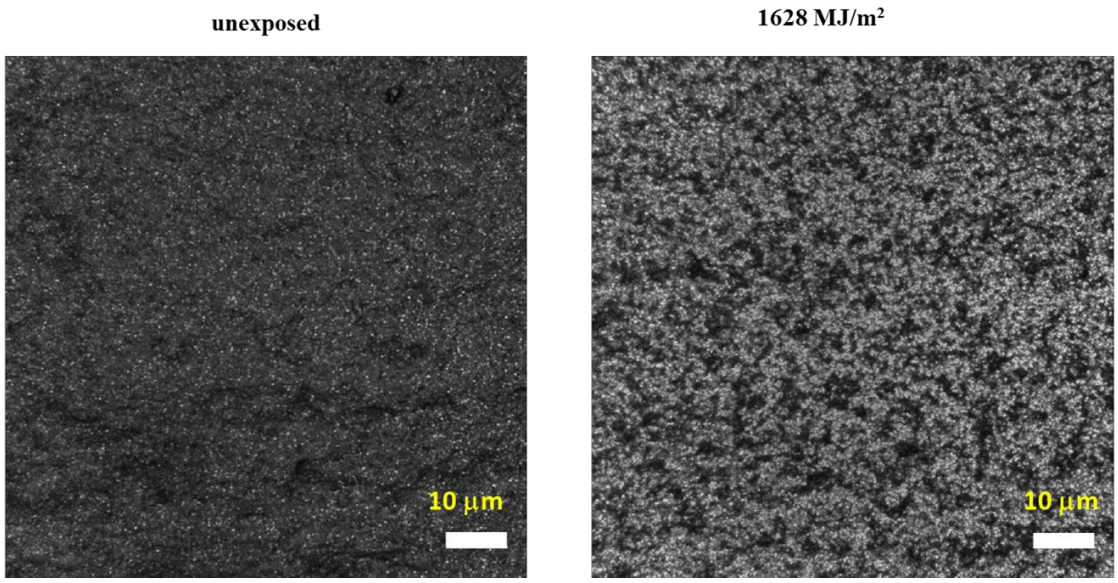


**Fig. 10. LSCM images of front U-PVC before and after exposure in SPHERE (1628 MJ/m$^2$, 55 °C, 75 % RH)**

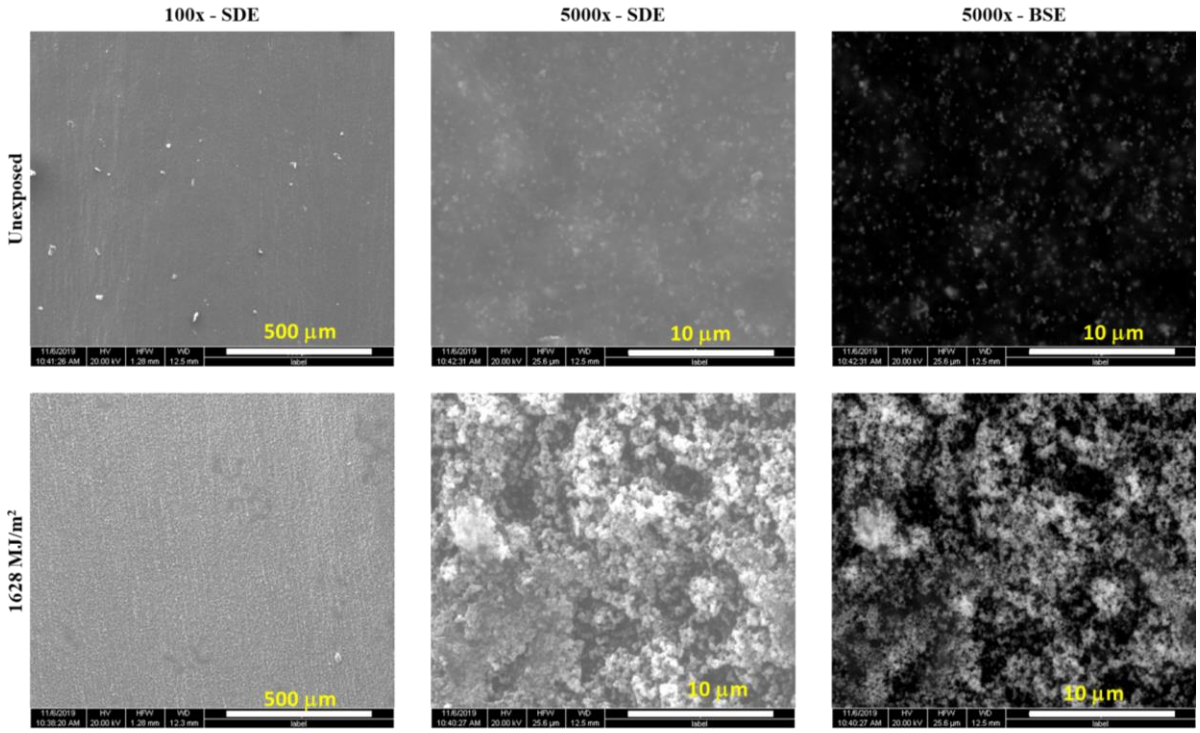


**Fig. 11. SEM images of front U-PVC before and after exposure in SPHERE (1628 MJ/m$^2$, 55 °C, 75 % RH). Here SDE presents secondary electron and BSE presents back scattering electron images.**

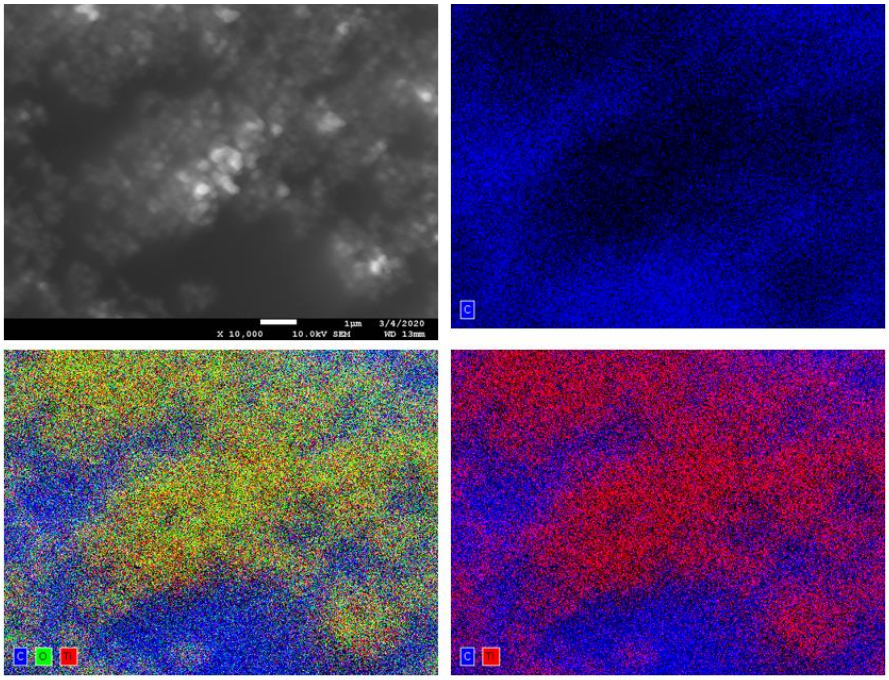

**Fig. 12. SEM of front U-PVC after SPHERE (1628 MJ/m$^2$, 55 °C, 75 % RH) (top-left) and relative EDX mapping for carbon only (top-right); carbon, oxygen and titanium (bottom-left); carbon and titanium (bottom-right).**

### 3.3.2. Mechanical properties

The overall effect of photo- and photo-catalyzed oxidation during weathering is mainly a chain scission reaction that reduces elongation at break and tensile strength. The chain scission reactions and the erosion of its products progressively reduce the thickness of the undegraded core and, thus, the mechanical properties of the item.

The tensile properties were affected by the orientation (either parallel or perpendicular) of the dogbone (DB) specimen *versus* the surface pattern (Fig. 13). For perpendicular-cut DBs, the elongation at break (EaB) varies from (0.32 ± 0.03) % before weathering to (0.2 ± 0.02) % after UV exposure (254 MJ/m$^2$). The EaB values (Fig. 13c) are slightly affected by UV dose. For parallel-cut DBs, the elongation at break (EaB) varies from (3.11 ± 0.3) % before weathering to (0.36 ± 0.06) % after UV exposure, and the EaB values change from over 300 % at 0 MJ/m$^2$ to 40 % at 254 MJ/m$^2$. Because parallel-cut DBs are more sensitive than perpendicular-cut DBs to weathering effects, parallel-cut DBs were used for the remainder of this study.

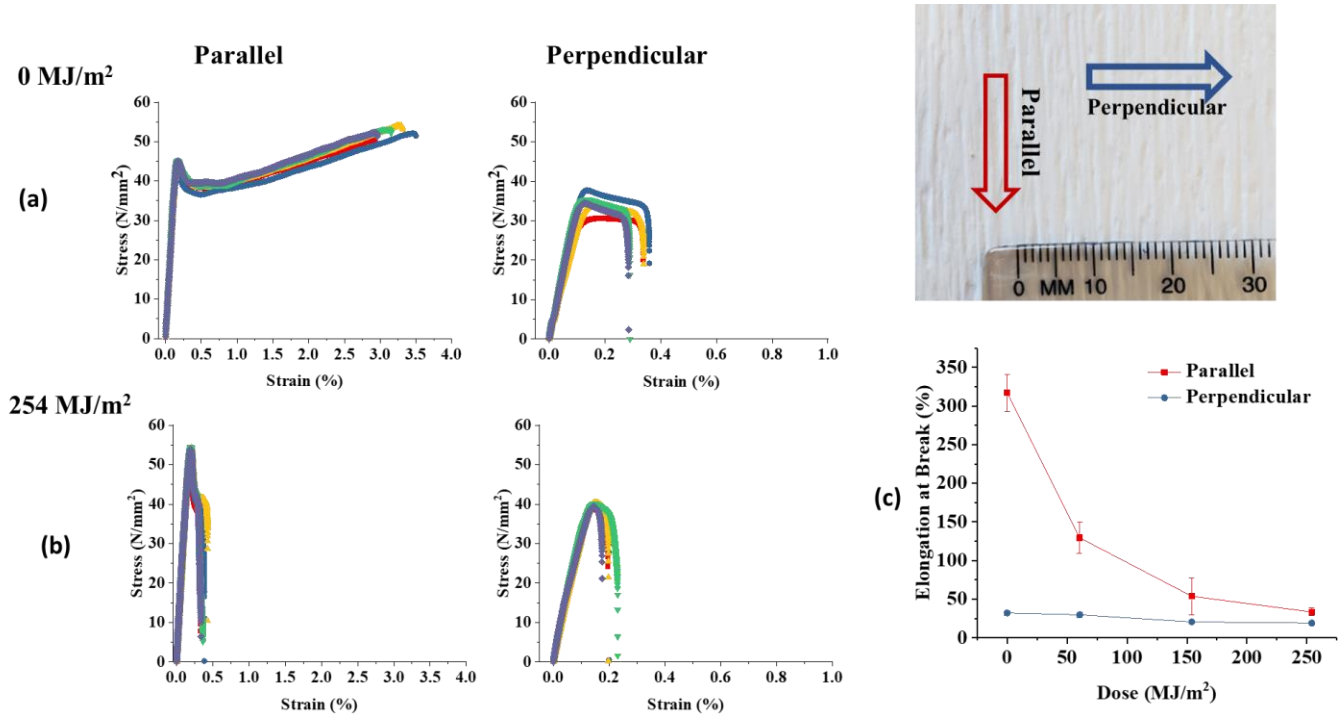


**Fig. 13. Tensile tests for dogbones cut parallel and perpendicular to the vinyl siding pattern direction: (a) stress-strain curves before weathering; (b) stress-strain curves after weathering (254 MJ/m$^2$); (c) elongation at break *vs*. dose. Data points indicate the mean and the error bars the standard deviation calculated over 5 replicates.**

The weathering conditions have a substantial impact on the mechanical properties, as shown in Fig. 14. The degradation rate of EaB: EaB (FL) << EaB (SPHERE 55 °C, 75 % RH) < EaB (SPHERE 70 °C, 75 % RH) ≅ EaB (QUV). The results of the QUV test at 60 °C with water condensation on the sample surface were similar to those at SPHERE 70 °C, 75 % RH conditions and provided much more damage than those at SPHERE 55 °C, 75 % RH. The effect of weathering conditions

on the mechanical properties is consistent with the impact of weathering conditions on chemical degradation and ΔYI (sections 3.2.1 and 3.2.2).

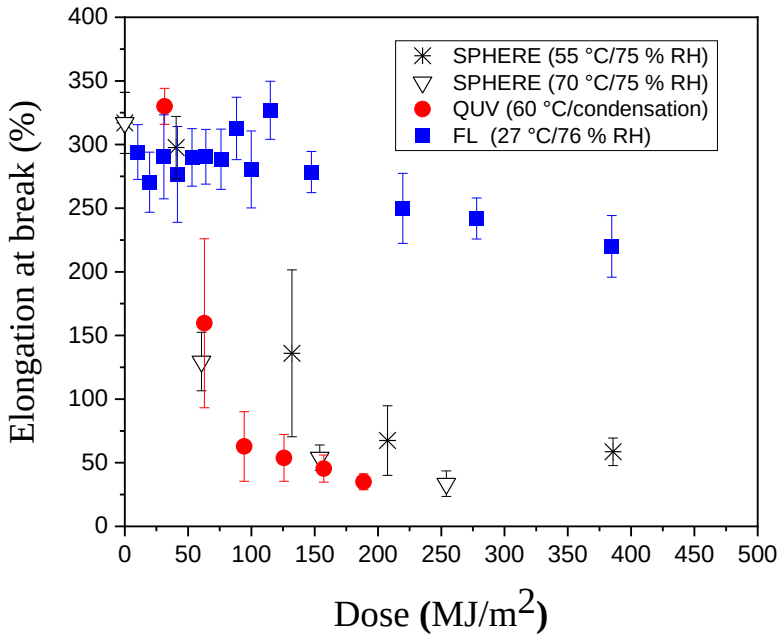


**Fig. 14. Elongation at break (EaB) of U-PVC under QUV exposure at four exposure conditions as indicated. The EaB values are average of 5 measurements and error bars represent one standard deviation.**

### 3.2. Weathering of research and development formulations (R&DF)

In R&DF, the type and quantity of additives were varied to study their impact on PVC weathering. Formulation A was designed to replicate a typical formulation used as a vinyl siding substrate beneath the capstock. This formulation lacks UV stabilizers and has minimal $TiO_2$, thus resulting in excellent initial color. Formulations C, F, and H were selected not as representative examples of U-PVC-based capstock but because they contained additives whose effects on U-PVC weathering were considered worthwhile investigating. These formulations provide an opportunity to explore the impact of various additives on the weathering characteristics of U-PVC materials, shedding light on how different formulations and compositions affect the long-term durability and performance of PVC-based products.

Formulation A(ref) contains a tin-based stabilizer and very low $TiO_2$ content. It is the most sensitive to weathering. Formulation C included chlorinated polyethylene (CPE) and acrylic impact modifier (AIM). It was used to investigate the effect of CPE on weathering. Formulation F closely resembled formulation C but with a higher AIM content and no CPE. This adjustment is intended to enhance weatherability (due to a significant amount of $TiO_2$ and the absence of CPE) while maintaining good mechanical properties (thanks to AIM). Formulation H was nearly identical to formulation F but contained a high filler content of calcium carbonate ($CaCO_3$). This

variation allowed us to study the impact of filler content on the weathering performance of the material, particularly in comparison to formulations C and F. All three formulations (C, F, and H) were stabilized with a calcium zinc stabilizer, a well-established additive used in EU for manufacturing weather-resistant products such as window profiles.

### 3.3.1. Effect of weathering on the chemistry of R&DF

Fig. 15 displays the FTIR spectra of all R&DF under QUV exposure conditions up to 12 weeks (353.8 MJ/m$^2$).

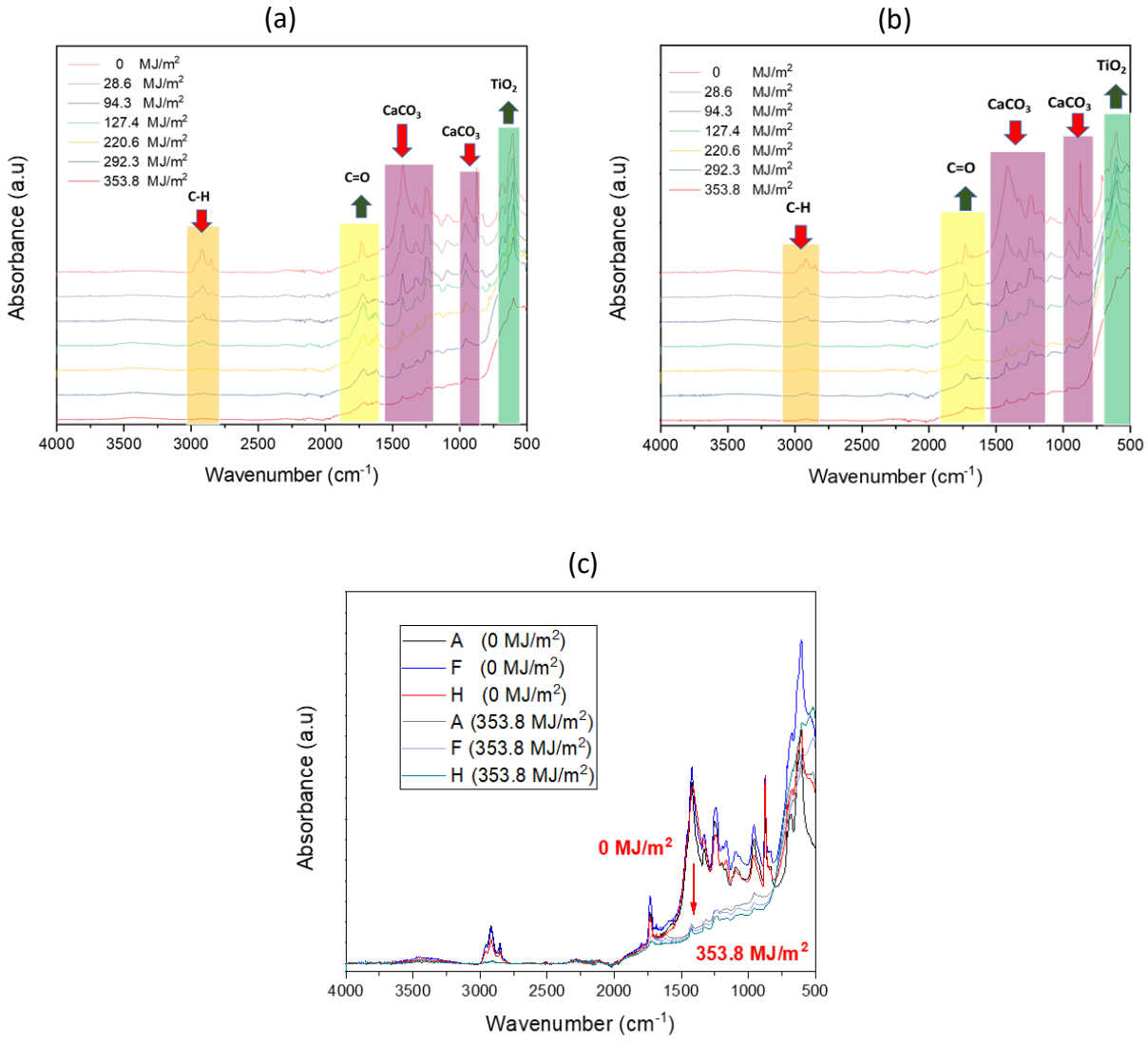


**Fig. 15: FTIR spectra after QUV exposure for: (a) formulation A at different exposure doses, (b) formulation H at different exposure doses, and (c) comparison of all formulations at 0 MJ/m$^2$ and 353.8 MJ/m$^2$.**

The common features observed in exposed samples as exposure times increase include:

- Decrease of the $CaCO_3$ bands (1434 $cm^{-1}$ – 880 $cm^{-1}$)
- Increase of $TiO_2$ broadband (790 $cm^{-1}$– 500 $cm^{-1}$)
- Decrease of C-H signal - (2700 $cm^{-1}$ – 3000 $cm^{-1}$)
- Increase and broadening of C=O band from (1731 to 1685) $cm^{-1}$.

The observed degradation patterns are consistent with the findings described in section 3.2.1. The FTIR-ATR analyzes from the surface to a depth of about 2 μm, where photo-oxidation and photo-catalyzed oxidation dominate. This phenomenon leads to oxidation and disintegration of the PVC matrix, as highlighted by the increase of the C=O signal and decrease of CH stretching. Another sign of surface degradation is the increase in the intensity of the $TiO_2$ bands (790 $cm^{-1}$ and 500 $cm^{-1}$), as seen in ASA capstock weathering in section 3.2.1. Furthermore, a collapse of the bands of $CaCO_3$ is also observed. This is a result of photo-degradation releasing HCl and then reacting with $CaCO_3$ to yield $CO_2$ and $CaCl_2$.

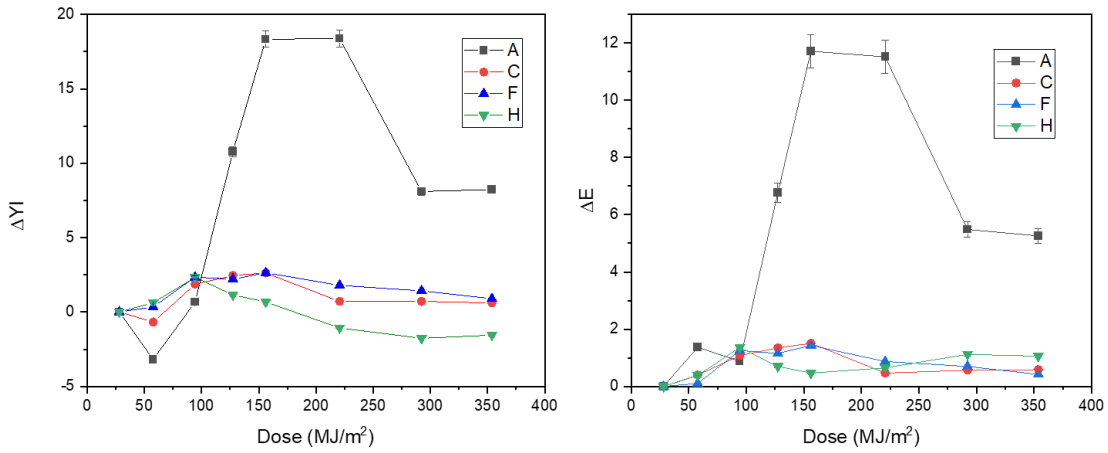


**Fig. 16: Color shift (ΔE) and yellowing (ΔYI) for formulation samples A, C, F, and H at different exposure doses under QUV exposure up to 12 weeks (353.8 MJ/m²). Data points indicate the mean. Error bars are the standard deviation values (5 replicates).**

The chemical alterations on the surface manifest themselves through the color changes of specimens during weathering (see Fig. 16). Formulation A, characterized by a lower $TiO_2$ content, exhibits a significant increase in both ΔYI and ΔE, indicating – as expected - a more pronounced degradation. The fluctuations observed in ΔYI and ΔE, particularly evident in $A_{ref}$, are attributed to cracks and holes generated by the breakdown of the matrix during weathering.

### 3.3.2. Effect of weathering on the mechanical properties of R&DF

As a result of weathering, the thickness of the undegraded U-PVC layer decreases over time, ultimately leading to the deterioration of the mechanical properties. To evaluate this effect on R&DF, the mechanical properties of specimens weathered in SPHERE (55 °C, 75% RH) were measured in terms of tensile impact strength test (ISO 8256). Fig. 17 compares the tensile impact strength for U-PVC and the R&DF (A, H, C, F) as a function of dose (see Table 1). Formulation A exhibits the worst behavior. Before weathering, formulation F, comprising only the acrylic impact modifier, a $TiO_2$ mass of 7.5 g per 100 g of PVC (hereafter, g of an additive per 100 g of PVC is referred to as phr) and a 15 phr $CaCO_3$ content, demonstrates the best initial mechanical properties, while Formulation H, with the highest $CaCO_3$ content (30 phr), performs the poorest. Formulation C, with less impact modifier, falls in between.

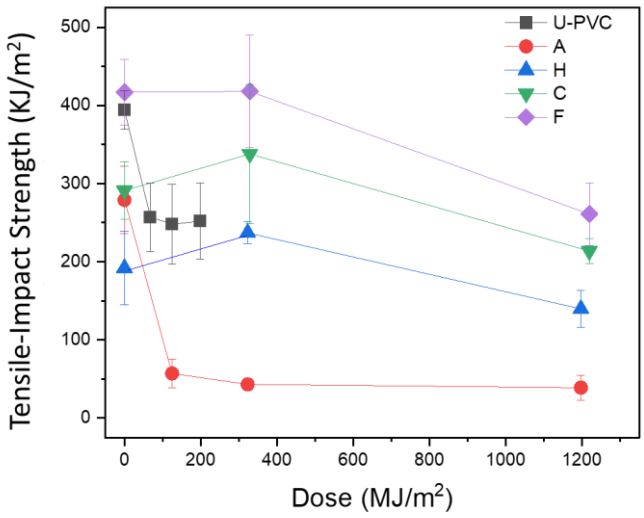


**Fig. 17: Impact strength tests for commercial U-PVC and R&DF. Weathering in SPHERE at 55 °C, 75 % RH. Data points indicate the mean and the error bars the standard deviation values (5 replicates).**

### 3.3.3. Fire performance of R&DF and effect of weathering

The MCC provided the heat release rate of each U-PVC formulation by pyrolyzing specimens in nitrogen and then oxidizing the pyrolizates in a combustion chamber at 900 °C. Pristine samples without weathering (A ref, C, F, and H) were run in triplicates. In contrast, only a single test was run for the weathered samples (A ref 378h, C 378h, F 378h, and H 378h). They were subjected to 387 h of accelerated aging in the SPHERE.

Representative heat release curves measured by MCC for the specimens before aging are shown in Fig. 18.

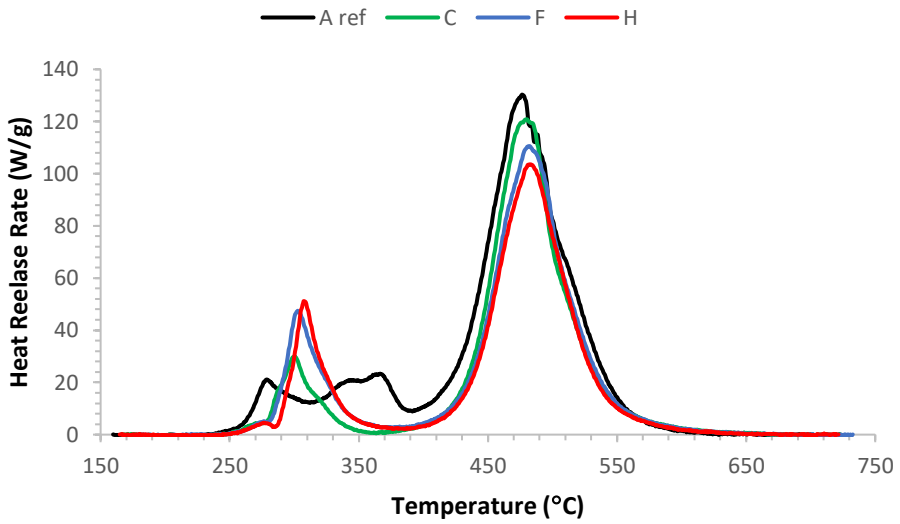


**Fig. 18: Representative heat release rate curves measured by MCC for the pristine specimens.**

The heat release curves indicate a two-stage decomposition mechanism [31-33, 49]. As discussed in these references, the first stage occurs between 230 °C and 390 °C generates a moderate heat release peak of about 20 W/g to 50 W/g. The second stage occurs between 410 °C and 570 °C and generates a more intense heat release peak of about 100 W/g to 140 W/g. The first decomposition step is associated with dehydrochlorination, i.e., the release of HCl and other hydrocarbons (e.g., benzene) in the gas phase. These reactions lead to a mass loss of about 60 % and the formation of conjugated polyene sequences and cross-linked structures. The second decomposition step is associated with chain scission of the cross-linked matrix, yielding tar and char formation.

Fig. 19 shows the heat release rate curves measured by MCC for the weathered specimens. No noticeable effect of weathering was observed when comparing the MCC curves for the pristine and aged samples.

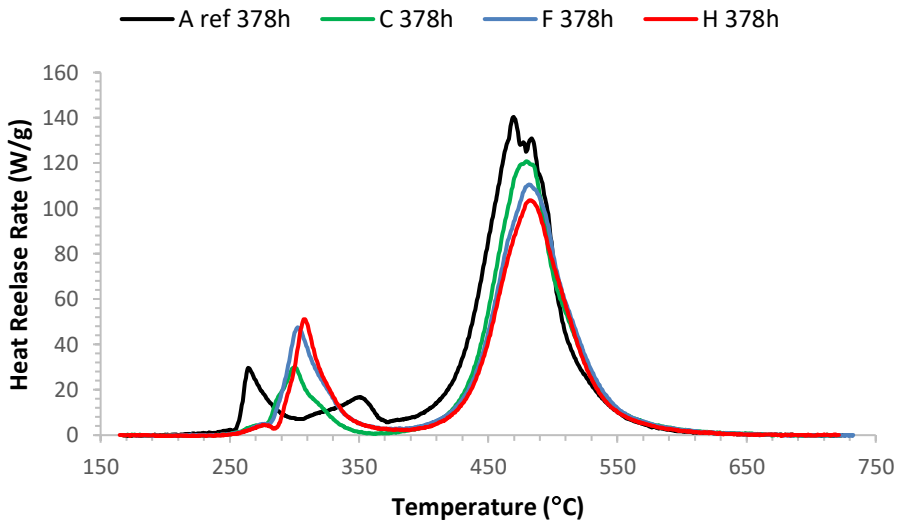


**Fig. 19: Heat release rate curves measured by MCC for the weathered specimens.**

MCC was used to rapidly screen the effect of formulation and weathering on the fire performance of U-PVC by using parameters such as residue, maximum heat release rate (Qmax), specific heat release ($h_c$), and fire growth capacity (FGC). These parameters were calculated according to ASTM D7309 method A. These data are summarized in Table 6.

**Table 6: Values of residue, maximum specific heat release rate (Qmax), specific heat release ($h_c$), and fire growth capacity (FGC) measured by MCC for each formulation.**

| Sample | Residue [%] | Qmax [W/g] | $h_c$ [kJ/g] | FGC [J/g-K] |
|---|---|---|---|---|
| A ref | 22.5 ± 0.2 | 134 ± 7 | 11.9 ± 0.2 | 93.3 ± 1.1 |
| A ref 378h | 23.0 | 139 | 11.1 | 88.0 |
| C | 31.7 ± 0.2 | 123 ± 2 | 9.1 ± 0.1 | 70.5 ± 0.8 |
| C 378h | 30.6 | 121 | 9.0 | 70.2 |
| F | 30.5 ± 0.2 | 114 ± 2 | 9.4 ± 0.2 | 73.5 ± 1.4 |
| F 378h | 30.6 | 111 | 9.4 | 72.8 |
| H | 32.8 ± 0.2 | 103 ± 1 | 8.5 ± 0.0 | 67.1 ± 0.8 |
| H 378h | 32.6 | 104 | 8.6 | 67.5 |

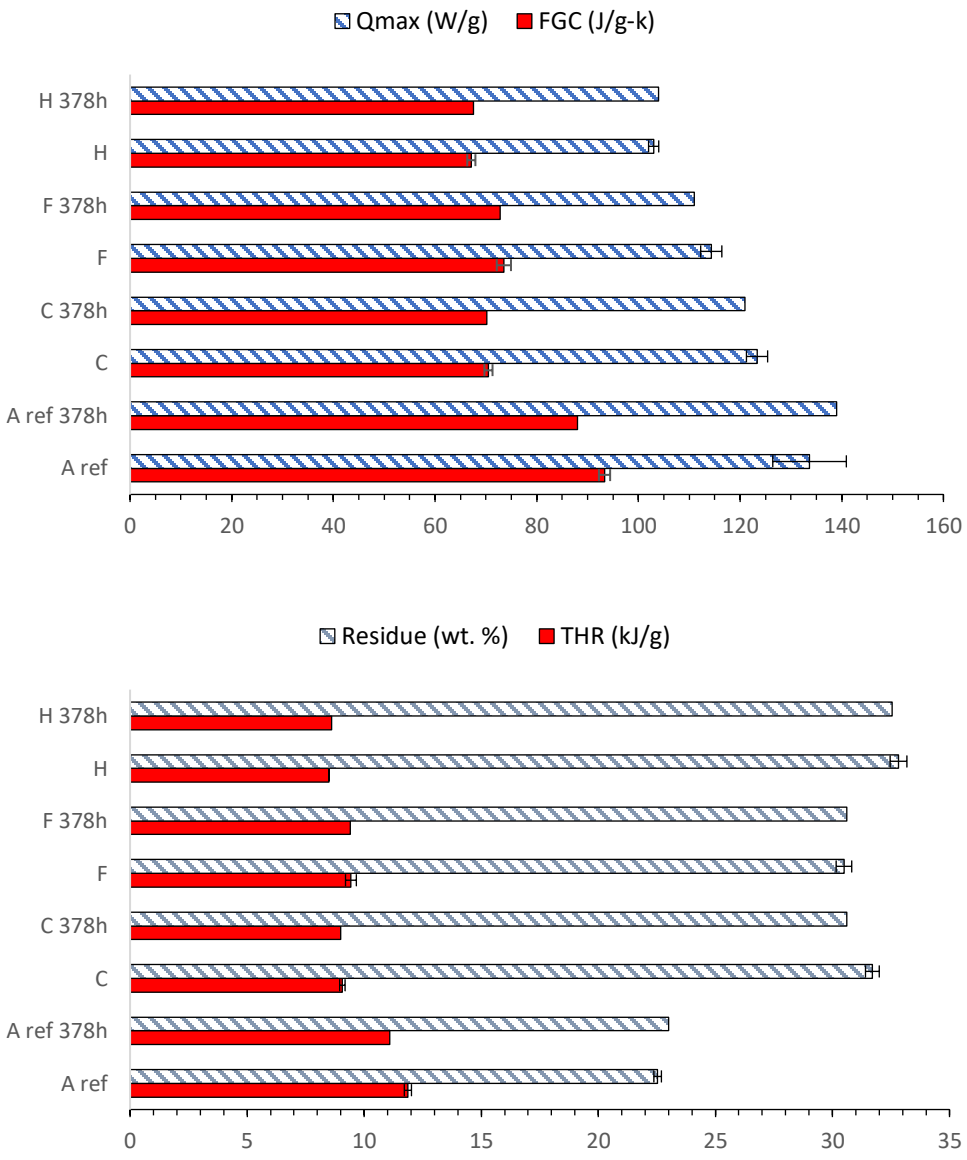


**Fig. 20: Bar chart comparing the performance parameters calculated in the MCC. Error bars are shown only for non-weathered samples as ± one standard deviation (three replicates).**

Among the pristine samples, Aref had the highest average FGC value (93.3 J/g-K), followed by F (73.5 ± 1.4 J/g-K), C (70.5 ± 0.8 J/g-K) and H (67.1 ± 0.8 J/g-K). A similar trend was observed for $h_c$ and FGC, whereas the trend was inverted for the residue. Based on a simple unpaired Student's t-test, these effects of formulation type on FGC are significant [50]. In particular, the decrease in FGC is highly statistically significant (two-tailed p-value < 0.0001) between A ref and C, statistically significant (p = 0.0322) between F and C, and very statistically significant (p = 0.0065) between C and H. For convenience, histograms for the data in Table 6 are shown in Fig. 20. The samples before weathering (A ref, C, F, and H) were run in triplicates. The samples

after weathering (A ref 378h, C 378h, F 378h, and H 378h) were run as a single test. Uncertainty is shown only for non-weathered samples as ± one standard deviation.

Considering MCC's limitations in predicting actual fire performance, these data suggest that sample H is expected to provide the best fire performance within the limited formulation tested. Compared to formulations C and F, formulation H had a 2x content of $CaCO_3$ (30 phr) and identical $TiO_2$ content (7.5 phr). The acrylic impact modifier content in formulation H (7.5 phr) was like that of formulation F and 3x that of formulation C, which also contained chlorinated polyethylene (see Table 1). These data suggest a marginal beneficial effect of $CaCO_3$ on PVC flammability. This result is somewhat surprising because the reaction of $CaCO_3$ with hydrogen chloride affects the flame-quenching mechanism. However, for calcium carbonate with a particle size in the micron range, the acid scavenging ability is low, and experimental data showed a slight increase in limiting oxygen index (LOI) when $CaCO_3$ was added into plasticized PVC (P-PVC) [31, 51]. Data also indicate that replacing 2.5 phr CPE in formulation C with 5.0 phr AIM in formulation F led to a significant increase in FGC from (70.5 ± 0.8) J/g-K to (73.5 ± 1.4) J/g-K. These data suggest that CPE provides a marginal but significant advantage in fire performance compared to AIM.

The weathering effect was estimated by comparing FGC values before and after weathering in Table 6 (e.g., H and H 378h). All formulations show no significant impact of weathering on FGC, except possibly for formulation A ref. However, because only single tests were run on weathered samples, further testing is required to validate the weathering impacts of FGC for formulation A ref.

The measured values of FGC and $h_c$ agree with previously reported data for U-PVC. [12, 52] For context, polyether ether ketone (PEEK) and polyethyleneimine (PEI), which are two performance polymers with very low flammability, have comparable values of FGC (80 J/g-K and 83 J/g-K, respectively) [12]. Hence, MCC data indicate an excellent fire performance for PVC. However, this does not imply that a U-PVC layer can act as a fire barrier, i.e., it can prevent flame penetration into an adjacent flammable substrate. As mentioned previously, MCC doesn't provide insight into heat/mass transfer due to the small sample size.

Understanding vinyl siding's ability to prevent flame penetration into an adjacent flammable insulation layer is of extreme interest for fire building safety, especially in areas subject to WUI fires. Furthermore, with the adoption of IECC 2021, exterior insulation will be required in U.S. climate zones (4 and above), where vinyl siding is often the most common siding material in residential buildings. To assess the barrier performance of the U-PVC formulations investigated in this study, a U-PVC sheet was placed on top of a 25 mm thick XPS foam insulation and tested according to ASTM E3367. The bottom of the assembly was open (see Fig. 1c) so that burn-through could be easily detected and the fire barrier performance among U-PVC formulations could be easily compared. The higher the barrier performance of U-PVC, the longer the burn-through time, as revealed by the ignition of the XPS foam.

Fig. **21** shows pictures captured during an ASTM E3367 test with the control U-PVC formulation, A ref. The first picture, at t = 0 s, shows the test assembly under the cone heater. The second picture with inset (t = 30 s) shows that the surface of U-PVC turns black due to charring; simultaneously, shrinkage and melting generate openings due to tearing on the perimeter of the specimen (see inset), exposing the underlying XPS foam and leading to XPS ignition within few seconds. The third picture (t = 40 s) shows an image of the specimen after the ignition of XPS foam, which rapidly melts and leads to a pool fire. Similar behavior was also observed for the other specimens with C, H, and F formulations, even though tearing on the surface of PVC and the consequent XPS ignition was further delayed compared to formulation A ref. The heat release curves measured with each formulation are shown in Fig. 22. For each test, there are two prominent peaks: the first is associated with the flaming of the U-PVC sheet, and the second with the flaming of XPS. The better the barrier performance of U-PVC, the longer the time elapsed between the two peaks. A ref had the worst barrier performance. All modified formulations showed improved barrier performance. Only single tests were run for each formulation. Multiple tests were not conducted in this study because none of the formulations was able to prevent ignition of XPS. Future work is required to improve the fire barrier performance of U-PVC.

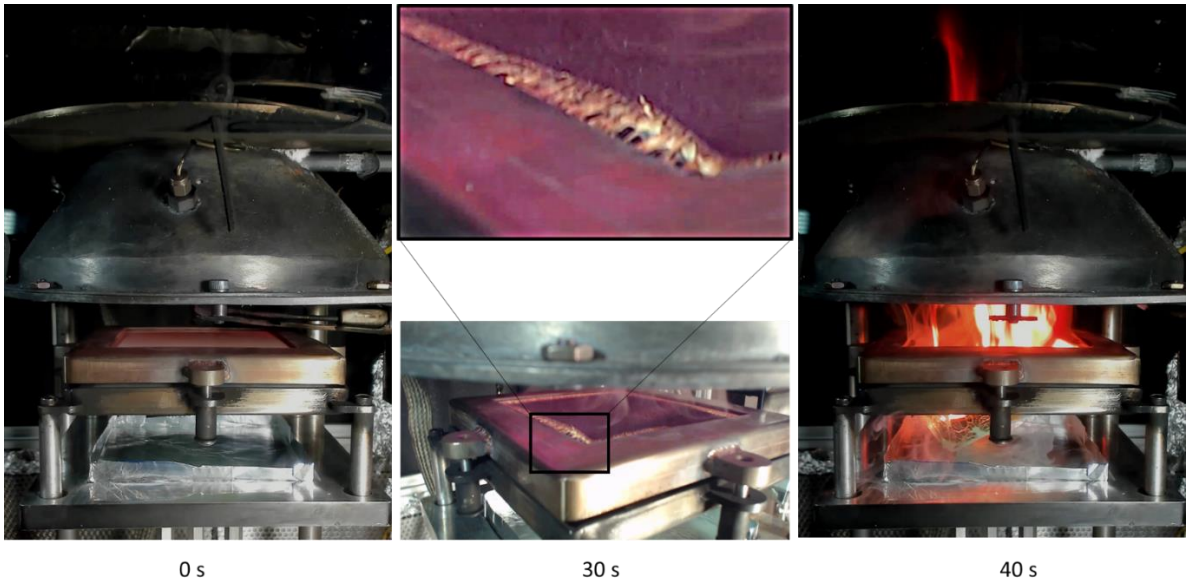


**Fig. 21: Pictures captured during an ASTM E3367 test with the control U-PVC formulation, A ref. At t = 0 s, the test assembly is exposed to the external heat flux (75 kW/m$^2$) generated by the cone heater. At t = 30 s, the surface of U-PVC turns black due to charring; simultaneously, shrinkage and melting generate openings on the perimeter of the specimen (see inset), leading to XPS ignition within few seconds. At t = 40 s, the specimen is flaming, and XPS rapidly melts leading to the formation of a pool fire.**

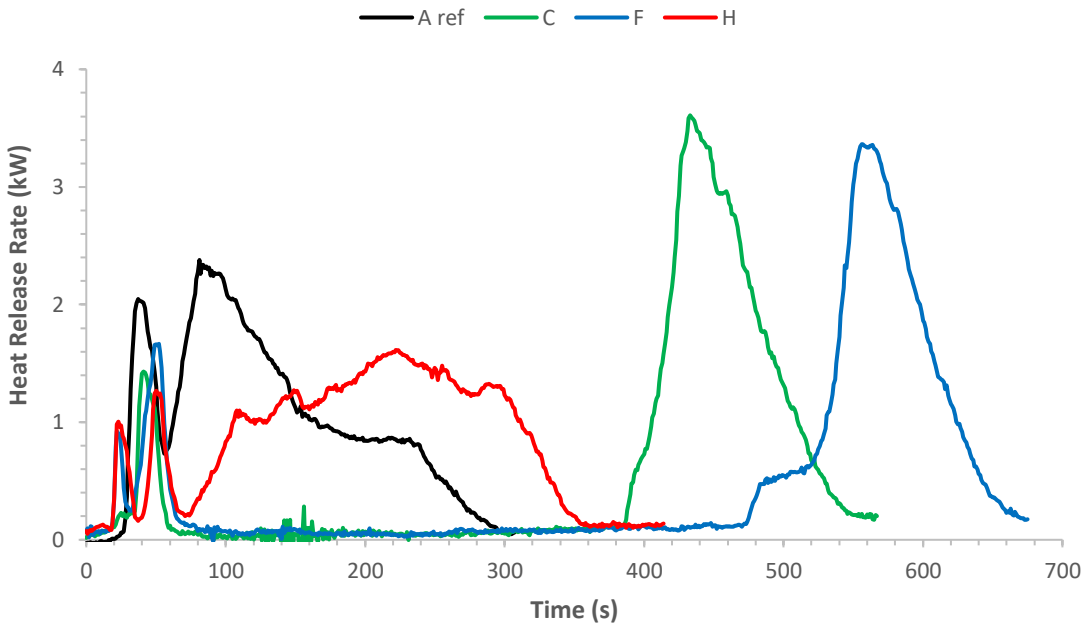


**Fig. 22: Heat release curves measured for assemblies of U-PVC and XPS sheets according to ASTM E3367.**

## 4. Conclusions

This study subjected a commercial vinyl siding with ASA capstock and lab-formulated U-PVC compounds to both natural and accelerated weathering (QUV and SPHERE) to investigate the chemical changes caused by weathering and its impact on aesthetic appearance, mechanical properties, and flammability.

Light absorption by ASA and PVC initiated a cascade of photochemical reactions that ultimately caused the polymeric matrix's disintegration. Weathering of the U-PVC formulation led to the release of HCl from the polymer backbone, the formation of polyene sequences with consequent yellowing and browning, the consumption of $CaCO_3$, and the gradual loss of the organic matrix with a resulting increase in $TiO_2$ concentration at the surface.

The ASA capstock is $TiO_2$ rich. This delayed the commercial vinyl siding weathering and remarkably improved its overall weatherability. The $TiO_2$ in the ASA capstock shielded the non-weatherable U-PVC substrate from degradation. However, over time, the breakdown of the polymeric matrix led to the formation of voids and clusters of $TiO_2$. This erosion exposed the underlying polymer to additional light degradation, compromising the mechanical properties.

In tensile tests, U-PVC samples showed a shift from ductile to brittle behavior with increasing UV exposure. Similarly, the extent of chemical degradation assessed by FTIR and yellowing, measured in terms of ΔYI, increased with the UV dose. This study also found that temperature and moisture content are critical factors influencing the degradation rates of elongation at break-in tensile tests. Therefore, when comparing and predicting the outdoor weathering of U-PVC using laboratory accelerated weathering tests, it is essential to consider the effects of these two key factors carefully.

The tensile impact tests confirmed the anticipated effects of additives — such as UV stabilizers, acrylic impact modifiers (AIM), $CaCO_3$ filler content, and $TiO_2$ content — on the mechanical impact strength (break energy) of U-PVC formulations. Formulation A demonstrated the poorest performance compared to Formulations H, C, and F. In contrast, Formulation F, which had high levels of AIM and $TiO_2$, exhibited the best performance.

Microscale combustion calorimetry showed that U-PVC formulations investigated here had a fire growth capacity between about 70 J/g-K and 90 J/g-K. These values are comparable to high-performance, low-flammability polymers like PEEK and PEI. The formulation type significantly affected the fire growth capacity. Specifically, formulation A ref showed the highest fire growth capacity (worst fire performance), followed by formulation F, C, and H (best fire performance). Adding calcium carbonate and replacing the acrylic impact modifier with chlorinated polyethylene reduced the fire growth capacity. Weathering in the SPHERE for 378 h did not

significantly affect fire growth capacity, except for a possible marginal effect on formulation A ref.

The fire barrier performance of U-PVC was investigated following protocols defined in ASTM E3367. All the U-PVC formulations investigated failed to protect the polystyrene foam substrate. The failure mechanism was identical in all formulations. It involved charring, shrinking, melting, and tearing on the surface of U-PVC, allowing flame penetration into the foam substrate. These results show that U-PVC is a remarkable inherently flame-retardant polymer but does not serve as an effective fire barrier. Further research is required to develop modified U-PVC formulations and building hardening solutions that may enable the use of vinyl siding in high-fire risk areas.

## 5. References


[1] Anonymous (2020) Residential Energy Consumption Survey (RECS). U.S. Energy Information Administration (EIA). Available on 09/12/2024 at https://www.eia.gov/consumption/residential/index.php.

[2] Anonymous (2021) 2021 International Energy Conservation Code (IECC). Available on 09/12/2024 at https://codes.iccsafe.org/content/IECC2021P2/chapter-1-ce-scope-and-administration.

[3] Abu-Jdayil B, Mourad A-H, Hittini W, Hassan M, Hameedi S (2019) Traditional, state-of-the-art and renewable thermal building insulation materials: An overview. *Construction and Building Materials* 214:709-735. https://doi.org/https://doi.org/10.1016/j.conbuildmat.2019.04.102

[4] Jelle BP (2011) Traditional, state-of-the-art and future thermal building insulation materials and solutions – Properties, requirements and possibilities. *Energy and Buildings* 43(10):2549-2563. https://doi.org/https://doi.org/10.1016/j.enbuild.2011.05.015

[5] Hirschler MM (2015) Flame retardants and heat release: review of data on individual polymers. *Fire and Materials* 39(3):232-258. https://doi.org/10.1002/fam.2242

[6] Ellis TM, Bowman DM, Jain P, Flannigan MD, Williamson GJ (2022) Global increase in wildfire risk due to climate-driven declines in fuel moisture. *Global change biology* 28(4):1544-1559.

[7] Anonymous (2023) Exterior Wall Materials. (United States Census Bureau).

[8] Weil ED, Levchik S, Moy P (2006) Flame and Smoke Retardants in Vinyl Chloride Polymers – Commercial Usage and Current Developments. *Journal of Fire Sciences* 24(3):211-236. https://doi.org/10.1177/0734904106057951

[9] (ISO) IOfS (2019)– *ISO/TR 20118:2019 - Plastics - Guidance on fire characteristics and fire performance of PVC materials used in building applications*), p 39.

[10] ASTM (2021)– *D7309 − 21b. Standard Test Method for Determining Flammability Characteristics of Plastics and Other Solid Materials Using Microscale Combustion Calorimetry* (ASTM International, West Conshohocken, PA).

[11] Safranova N, Lyon RE, Walters RN (2020) Microscale Fire Test for Component Substitutions in Aircraft Cabin Materials. (Federal Aviation Adinistration, Washington DC).

[12] Lyon RE, Safronava N, Crowley S, Walters RN (2021) A molecular-level fire growth parameter. *Polymer Degradation and Stability* 186:109478. https://doi.org/https://doi.org/10.1016/j.polymdegradstab.2020.109478

[13] ASTM (2023)– *ASTM E3367-23 Standard Test Method for Determining the Combustion Behavior of Layered Assemblies using a Cone Calorimeter*).

[14] Sonnier R (2022) Microscale forced combustion: Pyrolysis-combustion flow calorimetry (PCFC). *Analysis of Flame Retardancy in Polymer Science,* (Elsevier), pp 91-116.

[15] Lyon RE (2013) *Principles and Practice of Microscale Combustion Calorimetry*, (administration Fa).

[16] Zammarano M, Shields JR, Leventon I, Kim I, Nazare S, Thompson A, Davis RD, Chernovsky A, Bundy M (2021) Reduced-scale test to assess the effect of fire barriers on the flaming

combustion of cored composites: An upholstery-material case study. *Fire and Materials* 45(1):114-126. https://doi.org/https://doi.org/10.1002/fam.2910

[17] Zammarano M (2021) Technical Note (NIST TN) - 2194 Fire Performance of Upholstery Materials: Correlation between Cube Test and Full-Scale Chair Mock-Ups. (National Institute of Standards and Technology). https://doi.org/https://doi.org/10.6028/NIST.TN.2194

[18] Gugumus F (1985) Polymer light degradation. *Pastic Additives Handbook*, ed Gaechter RHM, H. (Carl Hanser Verlag, Munich), p 157.

[19] de Castro Monsores K, da Silva A, Oliveira S, Rodrigues J, Weber R (2019) Influence of ultraviolet radiation on polymethylmethacrylate (PMMA). *Journal of Materials Research and Technology* 8(5):3713-3718.

[20] Wypych G (2018) Data on specific polymers. *Handbook of material weathering,* (ChemTec Publishing), Chapter 14, Sixth Edition Ed., pp 369-590.

[21] Starnes Jr WH (2012) How and to what extent are free radicals involved in the nonoxidative thermal dehydrochlorination of poly (vinyl chloride)? *Journal of Vinyl and Additive Technology* 18(2):71-75.

[22] Decker C (1984) Degradation of poly (vinyl chloride) by UV radiation—II: mechanism. *European polymer journal* 20(2):149-155.

[23] Anton-Prinet C, Mur G, Gay M, Audouin L, Verdu J (1998) Photoageing of rigid PVC—I. Films containing CaZn thermal stabiliser. *Polymer degradation and stability* 60(2-3):265-273.

[24] Anton-Prinet C, Dubois J, Mur G, Gay M, Audouin L, Verdu J (1998) Photoageing of rigid PVC—II. Degradation thickness profiles. *Polymer degradation and stability* 60(2-3):275-281.

[25] Anton-Prinet C, Mur G, Gay M, Audouin L, Verdu J (1998) Photoageing of rigid PVC—III. Influence of exposure conditions on the thickness distribution of photoproducts. *Polymer degradation and stability* 60(2-3):283-289.

[26] Gardi S, Giannone L, Sarti G, Sarti G, Costa M (2023) Influence of initial season on PVC weathering. *Polymer Testing* 125:108123.

[27] Anton-Prinet C, Mur G, Gay M, Audouin L, Verdu J (1998) Photoageing of rigid PVC—IV. Effects of titanium dioxide. *Polymer degradation and stability* 61(2):211-216.

[28] Gardi S, Giannone L, Sarti G, Sarti G (2024) Surface Chalking upon Weathering of Dark-Colored PVC Articles and Relevant Stabilizers. *Polymers* 16(8):1047.

[29] Schiller M (2013) Uncharted Territory in the Use of PVC Products: Photo Effects. *PVC additives: Performance, Chemistry, Developments, and Sustainability*, ed Schiller M (Carl Hansen Verlag, Berlin), 1st Edition Ed., pp 281-367.

[30] Cho S , Choi W (2001) Solid-phase photocatalytic degradation of PVC–$TiO_2$ polymer composites. *Journal of Photochemistry and Photobiology A: Chemistry* 143(2-3):221-228.

[31] Bassi I, Delchiaro F, Bandinelli C, Mazzocchetti L, Salatelli E, Sarti G (2023) A New Perspective on Hydrogen Chloride Scavenging at High Temperatures for Reducing the Smoke Acidity of PVC Cables in Fires, IV: The Impact of Acid Scavengers at High Temperatures on Flame Retardance and Smoke Emission. *Fire* 6(7):259.

[32] Montaudo G , Puglisi C (1991) Evolution of aromatics in the thermal degradation of poly (vinyl chloride): a mechanistic study. *Polymer Degradation and Stability* 33(2):229-262.

[33] Anthony GM (1999) Kinetic and chemical studies of polymer cross-linking using thermal gravimetry and hyphenated methods. Degradation of polyvinylchloride. *Polymer degradation and stability* 64(3):353-357.

[34] Starns W , Edelson D (1979) Mechanistic aspects of the behavior of molybdenum (vi) oxide as a fire-retardant additive for poly (vinyl chloride). An interpretive review. *Macromolecules* 12(5):797-802.

[35] ASTM (2021)– *ASTM D 7793-21 Standard Specification for Insulated Vinyl Siding* (ASTM International, West Conshohocken, PA, USA).

[36] ASTM (2021)– *ASTM G7/G7M-2021. Standard Practice for Atmospheric Environmental Exposure Testing of Nonmetallic Materials* (ASTM International, West Conshohocken, PA).

[37] ASTM (2022)– *D638-22. Standard Test Method for Tensile Properties of Plastics* (ASTM International, West Conshohocken, PA).

[38] Chin J, Nguyen T, Byrd E, Martin J (2005) Validation of the reciprocity law for coating photodegradation. *JCT research* 2:499-508.

[39] Chin J, Byrd E, Embree N, Garver J, Dickens B, Finn T, Martin J (2004) Accelerated UV weathering device based on integrating sphere technology. *Review of scientific instruments* 75(11):4951-4959.

[40] ASTM (2023)– *ASTM G154-23 Standard Practice for Operating Fluorescent Ultraviolet (UV) Lamp Apparatus for Exposure of Materials* (ASTM International, West Conshohocken, PA, 2023).

[41] ASTM (2023)– *ASTM D2244-2316. Standard Practice for Calculation of Color Tolerances and Color Differences from Instrumentally Measured Color Coordinates* (ASTM International, West Conshohocken, PA).

[42] ASTM (2020)– *ASTM E313-20. Standard Practice for Calculating Yellowness and Whiteness Indices from Instrumentally Measured Color Coordinates*West Conshohocken, PA).

[43] ISO (2021)– *ISO 25178-2:2021 - Geometrical product specifications (GPS) — Surface texture: Areal — Part 2: Terms, definitions and surface texture parameters*).

[44] Park EJ, Park BC, Kim YJ, Canlier A, Hwang TS (2018) Elimination and Substitution Compete During Amination of Poly(vinyl chloride) with Ehtylenediamine: XPS Analysis and Approach of Active Site Index. *Macromolecular Research* 26(10):913-923. https://doi.org/10.1007/s13233-018-6123-z

[45] Zhang Y, Zhang X, Cao Y, Feng J, Yang W (2021) Acrylonitrile-styrene-acrylate particles with different microstructure for improving the toughness of poly (styrene-co-acrylonitrile) resin. *Advances in Polymer Technology* 2021:1-13.

[46] Rashidzadeh M (2008) Synthesis of High-Thermal Stable Titanium Dioxide Nanoparticles. *International Journal of Photoenergy*.

[47] Fang J, Xuan Y, Li Q (2010) Preparation of polystyrene spheres in different particle sizes and assembly of the PS colloidal crystals. *Science China Technological Sciences* 53:3088-3093.

[48] James S, Robinson A, Arnold J, Worsley D (2013) The effects of humidity on photodegradation of poly (vinyl chloride) and polyethylene as measured by the CO2 evolution rate. *Polymer degradation and stability* 98(2):508-513.

[49] Cruz PPR, da Silva LC, Fiuza-Jr RA, Polli H (2021) Thermal dehydrochlorination of pure PVC polymer: Part I—thermal degradation kinetics by thermogravimetric analysis. *Journal of Applied Polymer Science* 138(25):50598. https://doi.org/https://doi.org/10.1002/app.50598

[50] De Winter JCF (2019) Using the Student's t-test with extremely small sample sizes. *Practical Assessment, Research, and Evaluation* 18(1):10.

[51] Matthews G , Plemper GS (1981) Effects of calcium carbonate fillers on the behaviour of PVC in fires. *British Polymer Journal* 13(1):17-21. https://doi.org/https://doi.org/10.1002/pi.4980130105

[52] Guo H, Lyon RE, Safronava N (2018) Accuracy of heat-release rate measured in microscale combustion calorimetry. *Journal of Testing and Evaluation* 46(3):1090-1098.